Energy partition, scale by scale, in magnetic Archimedes Coriolis weak wave turbulence

A. Salhi, F. Baklouti, F. Godeferd, T Lehner, C. Cambon

Energy partition, scale by scale, in magnetic Archimedes Coriolis weak wave turbulence

A. Salhi,[1,2] F. S. Baklouti,[1] F. Godeferd,[2] T. Lehner,[3] and C. Cambon[2]

[1]*Département de Physique, Faculté des sciences de Tunis, 1060 Tunis, Tunisia*

[2]*Université de Lyon, Laboratoire de Mécanique des Fluides et d'Acoustique, UMR 5509, Ecole Centrale de Lyon, CNRS, UCBL, INSA F-69134 Ecully Cedex, France*

[3]*LUTH, UMR 8102 CNRS, Observatoire de Paris-Meudon, 5 place de Janssen, F-92195 Meudon, France*

(Received 7 August 2016; revised manuscript received 20 November 2016; published 22 February 2017)

Magnetic Archimedes Coriolis (MAC) waves are omnipresent in several geophysical and astrophysical flows such as the solar tachocline. In the present study, we use linear spectral theory (LST) and investigate the energy partition, scale by scale, in MAC weak wave turbulence for a Boussinesq fluid. At the scale k^{-1}, the maximal frequencies of magnetic (Alfvén) waves, gravity (Archimedes) waves, and inertial (Coriolis) waves are, respectively, $V_A k$, N, and f. By using the induction potential scalar, which is a Lagrangian invariant for a diffusionless Boussinesq fluid [Salhi *et al.*, Phys. Rev. E **85**, 026301 (2012)], we derive a dispersion relation for the three-dimensional MAC waves, generalizing previous ones including that of f-plane MHD "shallow water" waves [Schecter *et al.*, Astrophys. J. **551**, L185 (2001)]. A solution for the Fourier amplitude of perturbation fields (velocity, magnetic field, and density) is derived analytically considering a diffusive fluid for which both the magnetic and thermal Prandtl numbers are one. The radial spectrum of kinetic, $S_\kappa(k,t)$, magnetic, $S_m(k,t)$, and potential, $S_p(k,t)$, energies is determined considering initial isotropic conditions. For magnetic Coriolis (MC) weak wave turbulence, it is shown that, at large scales such that $V_A k/f \ll 1$, the Alfvén ratio $S_\kappa(k,t)/S_m(k,t)$ behaves like k^{-2} if the rotation axis is aligned with the magnetic field, in agreement with previous direct numerical simulations [Favier *et al.*, Geophys. Astrophys. Fluid Dyn. (2012)] and like k^{-1} if the rotation axis is perpendicular to the magnetic field. At small scales, such that $V_A k/f \gg 1$, there is an equipartition of energy between magnetic and kinetic components. For magnetic Archimedes weak wave turbulence, it is demonstrated that, at large scales, such that $(V_A k/N \ll 1)$, there is an equipartition of energy between magnetic and potential components, while at small scales $(V_A k/N \gg 1)$, the ratio $S_p(k,t)/S_\kappa(k,t)$ behaves like k^{-1} and $S_\kappa(k,t)/S_m(k,t) = 1$. Also, for MAC weak wave turbulence, it is shown that, at small scales $(V_A k/\sqrt{N^2+f^2} \gg 1)$, the ratio $S_p(k,t)/S_\kappa(t)$ behaves like k^{-1} and $S_\kappa(k,t)/S_m(k,t) = 1$.

DOI: 10.1103/PhysRevE.95.023112

I. INTRODUCTION

Magnetic Archimedes Coriolis (MAC) waves can occur in an electrically conducting fluid submitted to the Lorentz, buoyancy, and Coriolis forces. They are ubiquitously present in several geophysical and astrophysical systems (like the Earth's core, Sun's interior, solar corona, astrophysical accretion disks). These hydromagnetic waves are used to explain the secular variation of the Earth's magnetic field over the course of hundreds of years [1] and the redistribution of angular momentum in the Sun [2]. They also play an important role in the dynamo theory (see, e.g., Refs. [3–5]).

The interaction of magnetic (Alfvén) waves and inertial (Coriolis) waves in rapidly rotating fluid, which can generate slow and fast magnetic Coriolis (MC) waves, has been studied in some previous studies [5]. In the recent laboratory experiment of a magnetized turbulent Taylor-Couette flow of liquid metal by Nornberg *et al.* [6], the combined fast and slow magnetocoriolis waves were clearly identified where the observed slow MC wave is damped. These authors have identified a relationship between the slow MC wave and the magnetorotational instability (MRI) and proposed a method of determining the threshold for this instability through observation of driven MC waves. Note that the interaction of a background shear, which can be due to the differential rotation as in astrophysical accretion disks, with the MC (or MAC) waves can generate the MRI [7–10]. Salhi *et al.* [10] have found that the so-called "induction potential scalar," i.e., the inner product of the magnetic field by the gradient of the flow density, is a Lagrangian invariant for a diffusionless magnetized Boussinesq fluid, while its counterpart, i.e., the potential vorticity [11] is not a Lagrangian invariant for a magnetized fluid. With the help of that induction potential scalar, we derive a dispersion relation for three-dimensional MAC waves generalizing previous ones. For instance, Soward and Dormy [12], who follow Braginsky [13] in using a formulation in terms of the displacement vector of the wave perturbations, derived a dispersion relation for the MAC waves. Their formulation clearly shows that the MAC waves are associated with elliptical motion of particle. By ignoring the inertial term $(\partial \boldsymbol{u}/\partial t$, where $\boldsymbol{u}$ is the velocity perturbation field) in the linearized Boussinesq MHD equations for a diffusionless fluid, one can alternatively derive the Soward and Dormy's dispersion relation [5]. As noted by Finlay [5], ignoring the inertial term would have resulted in only the slow MAC mode being obtained, while the fast MAC mode [see Eq. (13)] is filtered out. We will show that the fast (respectively, slow) MAC mode propagates faster (respectively, slower) than the fast (slow) MC mode. Also, we briefly examine the similarity between the dispersion relation for the three-dimensional MAC waves and that of f-plane magnetohydrodynamic (MHD) "shallow water" waves [14–18]. The model has been applied to the solar tachocline [14]: a shear layer located inside the Sun at around $0.7R_\odot$, where $R_\odot$ is the solar radius, which contains a stably stratified sublayer (the radiative sublayer) that is around $0.02\ R_\odot$ deep [19].

The second aspect of the present study is to obtain analytical or semianalytical solutions of the linear equations in order to clarify the essential mechanisms governing the partition of energy, at each scale k^{-1} (or wave number k), between kinetic, magnetic, and potential components in MAC wave turbulence.

The case of MC weak wave turbulence is addressed in regards to the recent study by Favier *et al.* [20], who presented data from DNS of homogeneous incompressible turbulence submitted to both Coriolis and Lorentz forces (that are parallel) with large magnetic Reynolds number, moderate interaction parameter, and small Rossby number regime (context illustrated in Ref. [21]). In that study, it is found that the equipartition between kinetic and magnetic energy due to Alfvén waves (see Kraicknan [22]) is broken by inertial waves. This point is addressed in detail in the present study considering both cases where the uniform magnetic field and the system rotation axis are either parallel (axisymmetric case) or perpendicular (asymmetric case). The latter case being the most plausible configuration inside the Earth's core [23,24]. We show that the linear spectral theory (LST) results for the Alfvén energy ratio (kinetic and magnetic, e.g., see, Matthaeus and Goldstein [25]) are in agreement with the DNS ones. At large scales such that $V_A k/f \ll 1$, where V_A is the Alfvén velocity, the Alfvén ratio behaves like k^{-2} in the axisymmetric case and like k^{-1} in the asymmetric case. At small scales ($V_A k/f \gg 1$), LST predicts an equipartition of energy between kinetic and magnetic components in both the cases with or without rotation. Such a behavior at small scales would rather characterize the so-called weak MHD turbulence since nonrotating strong MHD turbulence submitted to uniform magnetic field is characterized by an Alfvén ratio slightly smaller than one, indicating the presence of non-Alfvénic fluctuations [25–27].

In a similar manner, we analyze the effects of linear processes on the energy partition, scale by scale, between kinetic, magnetic, and potential components in the MAC weak wave turbulence. We show that stratification affects the energy partition only at large scales ($V_A k/\sqrt{f^2+N^2} \ll 1$). At small scales ($V_A k/\sqrt{f^2+N^2} \gg 1$), stratification does not affect the equipartition of energy between magnetic and kinetic components, and the energy ratio potential/kinetic (or potential/magnetic) behaves like k^{-1}.

The paper is organized as follows. Governing Boussinesq MHD equations, as well as the equation for the induction potential scalar are presented in Sec. II. The linear differential system for the Fourier amplitudes is also derived and presented in Sec. II. The analysis of the dispersion relation for the MAC waves in the case of diffusionless fluid is given in Sec. III. Section IV deals with the analysis of the behavior, scale by scale, of the Alfvén ratio (kinetic/magnetic) in the case of MC weak wave turbulence. Similar analysis in the case of MAC wave weak turbulence is presented in Sec. V. Our concluding remarks are presented in Sec. VI. Some analytical developments are reported in Appendix.

II. GOVERNING EQUATIONS

A. The Boussinesq-MHD equations

We consider rotating homogeneous turbulence of an incompressible and conducting fluid submitted to a magnetic field and a vertical density stratification with uniform strength ($d\varrho/dx_3$). The system rotation $\boldsymbol{\Omega} = \frac{1}{2} f \boldsymbol{e}_3$, where $f = 2\Omega$ is the Coriolis parameter, is aligned with the vertical axis (x_3), while the magnetic field is either vertical $\boldsymbol{B} = B\boldsymbol{e}_3$ or horizontal $\boldsymbol{B} = B\boldsymbol{e}_1$. The temporal and spatial variations of the imposed field may be neglected so that, at least locally, we may assume that it is uniform and steady [28].

The fluctuating parts of the velocity, magnetic, and density fields are denote by $\boldsymbol{u} = (u_1,u_2,u_3)^T$, $\boldsymbol{b} = (b_1,b_2,b_3)^T$, and ρ, respectively.

We start from the usual Boussinesq MHD equations [21],

$$\begin{aligned}
\partial_t \boldsymbol{u} + (\boldsymbol{u}\cdot\boldsymbol{\nabla})\boldsymbol{u} &= -\frac{1}{\varrho_0}\boldsymbol{\nabla} p - 2\boldsymbol{\Omega}\times\boldsymbol{u} - \frac{g}{\varrho_0}\rho\boldsymbol{e}_3 \\
&\quad + \frac{1}{\varrho_0\mu_0}(\boldsymbol{\nabla}\times\boldsymbol{b})\times(\boldsymbol{B}+\boldsymbol{b}) + \nu\nabla^2\boldsymbol{u}, \\
\partial_t \boldsymbol{b} + (\boldsymbol{u}\cdot\boldsymbol{\nabla})\boldsymbol{b} &= ((\boldsymbol{B}+\boldsymbol{b})\cdot\boldsymbol{\nabla})\boldsymbol{u} + \eta\nabla^2\boldsymbol{b}, \\
\partial_t \rho + (\boldsymbol{u}\cdot\boldsymbol{\nabla})\rho &= -\frac{d\varrho}{dx_3}u_3 + \kappa\nabla^2\rho
\end{aligned} \tag{1}$$

where both $\boldsymbol{u}$ and $\boldsymbol{b}$ are solenoidal, so that $\boldsymbol{\nabla}\cdot\boldsymbol{u} = 0$ and $\boldsymbol{\nabla}\cdot\boldsymbol{b} = 0$. Here, ν, η, and κ denote the kinematic viscosity, magnetic diffusivity, and thermal diffusivity, respectively, and μ_0 is the vacuum permeability, while p denotes the pressure fluctuation, and ϱ is the background density and ϱ_0 is a reference density. Herein after, the tildes refer to instantaneous (total) quantities, e.g., $\tilde{\boldsymbol{b}} = \boldsymbol{B} + \boldsymbol{b}$.

It should be noticed that the so called induction potential scalar,

$$\begin{aligned}
\tilde{\varpi}_m &= \tilde{\boldsymbol{b}}\cdot\boldsymbol{\nabla}\tilde{\varrho} = (\boldsymbol{B}+\boldsymbol{b})\cdot(\boldsymbol{\nabla}\varrho + \boldsymbol{\nabla}\rho) \\
&= \underbrace{\boldsymbol{B}\cdot\boldsymbol{\nabla}\varrho}_{\varpi_m^{(m)}} + \underbrace{(\boldsymbol{B}\cdot\boldsymbol{\nabla}\rho + \boldsymbol{b}\cdot\boldsymbol{\nabla}\varrho)}_{\varpi_m^{(\ell)}} + \underbrace{\boldsymbol{b}\cdot\boldsymbol{\nabla}\rho}_{\varpi_m^{(n\ell)}},
\end{aligned} \tag{2}$$

is a relevant parameter when considering a magnetized Boussinesq fluid (see Salhi *et al.* [10]). Here, $\varpi_m^{(m)}$ represents the mean part of the total induction potential $\tilde{\varpi}$, while the last two terms, $\varpi_m^{(\ell)}$ and $\varpi_m^{(n\ell)}$, characterize the interaction between the mean and the fluctuating parts and the nonlinear interaction. The equation for $\tilde{\varpi}_m$, which is deduced from the Boussinesq MHD equations, reads

$$(\partial_t + (\tilde{\boldsymbol{u}}\cdot\boldsymbol{\nabla}))\tilde{\varpi}_m = \eta(\boldsymbol{\nabla}\tilde{\varrho})\cdot\nabla^2\tilde{\boldsymbol{b}} + \kappa\tilde{\boldsymbol{b}}\cdot\nabla^2(\boldsymbol{\nabla}\tilde{\varrho}). \tag{3}$$

Therefore, in the inviscid and nondiffusive limit, $\tilde{\varpi}_m$ is a Lagrangian invariant, while its counterpart, i.e., the potential vorticity [11], $\tilde{\varpi}_\kappa = (\boldsymbol{\nabla}\times\tilde{\boldsymbol{u}} + 2\boldsymbol{\Omega})\cdot\boldsymbol{\nabla}\tilde{\varrho}$, is not a Lagrangian invariant for a magnetized fluid [10]. Obviously, fluids in the tachocline or elsewhere are not perfectly inviscid, nor perfectly conducting but in some astrophysical flows as the solar tachocline, the high values of magnetic and hydrodynamic Reynolds numbers indicate that the effects of viscosity and magnetic diffusion are very low [19]. Accordingly, for mathematical simplicity, in the present study, we consider either a diffusionless fluid or a diffusive fluid for which the magnetic and thermal Prandtl numbers are unity ($\nu = \eta = \kappa$).

B. Spectral decompositions

We linearize Eqs. (1) and introduce the following spectral decompositions [29,30]:

$$\left(\boldsymbol{u},\frac{p}{\varrho_0},\frac{\boldsymbol{b}}{\sqrt{\varrho_0\mu_0}},-\frac{g}{\varrho_0}\rho\right)=\sum_{\boldsymbol{k}}(\hat{\boldsymbol{u}},\hat{p},\hat{\boldsymbol{b}},\hat{\rho})(\boldsymbol{k},t)\mathrm{e}^{\mathrm{i}\boldsymbol{x}\cdot\boldsymbol{k}}, \quad (4)$$

where $\boldsymbol{k}=(k_1,k_2,k_3)^T$ is the wave vector. We obtain a set of ordinary differential equations (spectral linear theory (SLT) equations, also called rapid distortion theory (RDT) equations [29,31]):

$$\begin{aligned}&\dot{\hat{\boldsymbol{u}}}+\nu k^2\hat{\boldsymbol{u}}=-\mathrm{i}\hat{P}\boldsymbol{k}-2\boldsymbol{\Omega}\times\hat{\boldsymbol{u}}+\hat{\rho}\boldsymbol{e}_3+\mathrm{i}(\boldsymbol{V}_a\cdot\boldsymbol{k})\hat{\boldsymbol{b}},\\&\dot{\hat{\boldsymbol{b}}}+\eta k^2\hat{\boldsymbol{b}}=\mathrm{i}(\boldsymbol{V}_a\cdot\boldsymbol{k})\hat{\boldsymbol{u}},\\&\dot{\hat{\rho}}+\kappa k^2\hat{\rho}=-N^2\hat{u}_3,\end{aligned} \quad (5)$$

with $\boldsymbol{k}\cdot\hat{\boldsymbol{u}}=0$ and $\boldsymbol{k}\cdot\hat{\boldsymbol{b}}=0$ for solenoidal fields, where $\boldsymbol{V}_a=(1\sqrt{\rho\mu_0})\boldsymbol{B}$ is the Alfvén velocity vector, $\hat{P}=(\hat{p}+(\boldsymbol{V}_a\cdot\hat{\boldsymbol{b}}))$ and N, such that $N^2=-(g/\varrho_0)(d\varrho/dx_3)$ is the Brunt-Väisälä frequency assumed to be a positive constant (stable stratification) in the present study.

The equation of the spectral counterpart of the linear part of the induction potential scalar, $\hat{\varpi}_m^{(\ell)}=\mathrm{i}(\boldsymbol{V}_a\cdot\boldsymbol{k})\hat{\rho}+N^2\hat{b}_3$, can be deduced either from Eq. (3) or from system Eq. (5),

$$\dot{\hat{\varpi}}_m^{(\ell)}=-\eta k^2\hat{\varpi}_m^{(\ell)}-(\kappa-\eta)k^2\mathrm{i}(\boldsymbol{V}_a\cdot\boldsymbol{k})\hat{\rho}, \quad (6)$$

where $k=\|\boldsymbol{k}\|$ is the modulus of the wave vector. For a diffusionless fluid, $\hat{\varpi}_m^{(\ell)}$ is time-independent and constitutes a constant of motion, as indicated previously. In the case where $\eta=\kappa$, Eq. (6) becomes autonomous with solution $\hat{\varpi}_m^{(\ell)}(t)=\hat{\varpi}_m^{(\ell)}(0)\exp(-\eta k^2 t)$.

Since $\boldsymbol{u}$ and $\boldsymbol{b}$ are solenoidal, the seventh-differential system Eq. (3) can be reduced to a fifth-dimensional one. In the present study, we transform the system Eq. (3) in a local frame, referred to as Craya-Herring in hydroturbulence [32], in which both the constraints $\boldsymbol{k}\cdot\hat{\boldsymbol{u}}=0$ and $\boldsymbol{k}\cdot\hat{\boldsymbol{b}}=0$ are satisfied by construction. Velocity and magnetic modes are constructed in a similar way as

$$\begin{aligned}&u^{(1)}=k_h^{-1}(k_2\hat{u}_1-k_1\hat{u}_2),\quad u^{(2)}=-k_h^{-1}k\hat{u}_3,\\&u^{(3)}=\mathrm{i}k_h^{-1}(k_2\hat{b}_1-k_1\hat{b}_2),\quad u^{(4)}=-\mathrm{i}k_h^{-1}k\hat{b}_3,\end{aligned} \quad (7)$$

($u^{(1)}$ and $u^{(3)}$) correspond to toroidal modes in physical space, and ($u^{(2)}$ and $u^{(4)}$) correspond to poloidal modes in physical space [33], where $k_h=\sqrt{k_1^2+k_2^2}$ denotes the horizontal wave number. In addition, the buoyancy mode is rescaled as a velocity, $u^{(5)}=N^{-1}\hat{\rho}$. Therefore, $\hat{\varpi}_m^{(\ell)}$ can be rewritten in terms of $u^{(4)}$ and $u^{(5)}$ as

$$-\mathrm{i}N^{-1}\hat{\varpi}_m^{(\ell)}=\omega_G u^{(4)}+\omega_A u^{(5)}, \quad (8)$$

in which

$$\omega_G=k_h k^{-1}N,\quad \omega_A=\boldsymbol{V}_a\cdot\boldsymbol{k}, \quad (9)$$

are, respectively, the frequencies of gravity (Archimedes) and magnetic (Alfvén) waves.

With the help of the induction potential scalar $\hat{\varpi}_m^{(\ell)}$, which constitutes a constant of motion for a diffusionless fluid, as already indicated, the fifth-dimensional linear differential system for the toroidal, poloidal, and buoyancy modes can be transformed into a fourth-dimensional inhomogeneous one,

$$\begin{pmatrix}\dot{u}^{(1)}\\\dot{u}^{(2)}\\\dot{u}^{(3)}\\\dot{u}^{(4)}\end{pmatrix}=\begin{pmatrix}0&\omega_R&\omega_A&0\\-\omega_R&0&0&-\frac{\omega_{AG}^2}{\omega_A}\\-\omega_A&0&0&0\\0&\omega_A&0&0\end{pmatrix}\cdot\begin{pmatrix}u^{(1)}\\u^{(2)}\\u^{(3)}\\u^{(4)}\end{pmatrix}+\begin{pmatrix}0\\\pi^{(0)}\\0\\0\end{pmatrix}. \quad (10)$$

The solution of system Eq. (10) that characterizes an inviscid fluid ($\nu=\eta=\kappa=0$) is reported in Appendix A for the sake of clarity [see Eqs. (A2), (A7), (A8)]. By multiplying the solution derived in the inviscid case by the damping term $\mathrm{e}^{-\nu k^2 t}$, we obtain the solution for a diffusive fluid with $P_{rm}=\nu/\eta=1$ and $P_{rt}=\nu/\kappa=1$.

The frequencies,

$$\omega_R=f\frac{k_3}{k},\quad \omega_{AG}=\sqrt{\omega_A^2+\omega_G^2}, \quad (11)$$

appearing in system Eq. (10) are, respectively, the frequencies of Coriolis waves and magnetic Archimedes waves, and

$$\pi^{(0)}=-\mathrm{i}\frac{\omega_G}{N\omega_A}\hat{\varpi}_m^{(\ell)}=\frac{\omega_G}{\omega_A}(\omega_G u^{(4)}(\boldsymbol{k},0)+\omega_A u^{(5)}(\boldsymbol{k},0)) \quad (12)$$

is a constant depending only on the initial energy distribution. Note that both ω_R and ω_G depend on the orientation of the wave vector and not on its modulus, i.e., there is no dependence on the wavelength, $\lambda=2\pi/k$, while the Alfvén frequency does depend on λ.

III. DISPERSION RELATIONS FOR A DIFFUSIONLESS FLUID

In order to focus on the essential physics involving the Lorentz (magnetic), buoyancy (Archimedes), and Coriolis forces, we ignore viscous, magnetic, and thermal diffusion and derive a dispersion relation for three-dimensional MAC waves.

We determine the eigenvalues of the above coefficient matrix that are the solutions of the following algebraic firth-order equation:

$$\left(\omega^2-\omega_A^2\right)\left(\omega^2-\omega_A^2-\omega_G^2\right)-\omega^2\omega_R^2=0. \quad (13)$$

Equation (13) provides the dispersion relation for the MAC waves in a diffusionless fluid. For a diffusive fluid with $\nu=\eta=\kappa$, the dispersion relation of the MAC waves is obtained by replacing ω in Eq. (13) by $(\omega-\nu)$. We can gain insight into the basic waves for this dispersion relation by examining some limiting cases.

In the absence of stratification, Eq. (13) reduces to

$$\left(\omega^2-\omega_R\omega-\omega_A^2\right)\left(\omega^2+\omega_R\omega-\omega_A^2\right)=0, \quad (14)$$

which describes both fast and slow magnetic Coriolis waves for a diffusionless fluid [5]. For these waves, the Lorentz and Coriolis forces may act together, stiffening the system and producing the higher-frequency fast wave, or the two forces

may oppose one another to produce the lower-frequency slow wave [6],

$$\begin{aligned}\omega_f &= \tfrac{1}{2}\left(\sqrt{\omega_R^2+4\omega_A^2}+\omega_R\right),\\ \omega_s &= \tfrac{1}{2}\left(\sqrt{\omega_R^2+4\omega_A^2}-\omega_R\right),\end{aligned} \tag{15}$$

using subscripts s and f for "slow" and "fast," respectively. We remark that fast and slow magnetic Coriolis waves for a diffusionless fluid are associated to the following modes:

$$\begin{aligned}\Psi_f &= \left(\omega_f^2-\omega_s^2\right)^{-1}\Big[\omega_A\omega_R u^{(1)} - \mathrm{i}\frac{\omega_A}{\omega_f}\left(\omega_A^2+\omega_R^2-\omega_s^2\right)u^{(2)}\\ &\quad -\mathrm{i}\frac{\omega_R}{\omega_f}\omega_A^2 u^{(3)} + \left(\omega_A^2-\omega_s^2\right)u^{(4)}\Big],\\ \Psi_s &= \left(\omega_s^2-\omega_f^2\right)^{-1}\Big[\omega_A\omega_R u^{(1)} - \mathrm{i}\frac{\omega_A}{\omega_s}\left(\omega_A^2+\omega_R^2-\omega_f^2\right)u^{(2)}\\ &\quad -\mathrm{i}\frac{\omega_R}{\omega_s}\omega_A^2 u^{(3)} + \left(\omega_A^2-\omega_s^2\right)u^{(4)}\Big],\end{aligned} \tag{16}$$

for which the dynamical system Eq. (10) with $\omega_G = 0$ is transformed to a simple decoupled system,

$$\dot{\Psi}_f = \mathrm{i}\omega_f\Psi_f, \quad \dot{\Psi}_s = \mathrm{i}\omega_s\Psi_s. \tag{17}$$

From the later equation, one easily verifies that the total (kinetic+magnetic) energy, $\mathcal{E}_t = |\Psi_f|^2 + |\Psi_s|^2$, is conserved (in the inviscid linear limit). Note that, scale by scale, the relative importance of rotation and magnetic tension can be estimated from the ratio $\omega_A/\omega_R = V_A k/f$.

In the absence of rotation, the dispersion relation Eq. (13) reduces to

$$\left(\omega^2-\omega_A^2\right)\left(\omega^2-\omega_A^2-\omega_G^2\right) = 0, \tag{18}$$

which indicates that the toroidal modes $u^{(1)}$ and $u^{(3)}$ propagate with the Alfvén frequency ω_A, while the poloidal and buoyancy modes $u^{(2)}$, $u^{(4)}$, and $u^{(5)}$ propagate with the frequency $\omega_{AG} \geqslant \omega_A$. Accordingly, for the motion of the poloidal and buoyancy modes, both the gravity and the magnetic tension contribute to the restoring force on a displaced fluid element, so the wave is a mixture of gravity and Alfvén waves [34]. The ratio $\omega_A/\omega_G = V_A k/N$ characterizes, scale by scale, the importance of the magnetic tension with respect to the gravity force. In the solar tachocline, the lowest value of the ratio $V_A k/N$ would be $V_A k/N \sim 10^{-2}$ for $k^{-1} \sim (0.02 \times R_\odot)$, $V_A = 13\,\mathrm{m.s^{-1}}$ and $N = 8\times 10^{-5}\ \mathrm{s^{-1}}$ (see Ref. [19]).

In the case of small Alfvén speed ($V_A \ll NL_0$ with L_0 a characteristic length scale), as in the interiors of solar-like stars [16] or at vanishing magnetic field, the dispersion relation Eq. (13) reduces to $\omega = \sqrt{\omega_G^2+\omega_R^2}$, which describes Archimedes Coriolis (AC) waves. Let $\lambda_R = NL_0/f$ be the Rossby-deformation radius [35]. The rotational effects become important at wavelengths of $\lambda \equiv k^{-1} \gtrsim \lambda_R$ [17]. Note that the case of stratified rotating homogeneous turbulence involving AC waves has been addressed in previous studies [21,33,36].

When rotation, stratification, and magnetic fields are simultaneously present, the solution of the dispersion relation Eq. (13) characterizes fast and slow waves with frequency,

$$\begin{aligned}\omega_F^2 &= \frac{1}{2}\left[2\omega_A^2+\omega_G^2+\omega_R^2+\sqrt{\left(\omega_R^2+\omega_G^2\right)^2+4\omega_A^2\omega_R^2}\,\right],\\ \omega_S^2 &= \frac{1}{2}\left[2\omega_A^2+\omega_G^2+\omega_R^2-\sqrt{\left(\omega_R^2+\omega_G^2\right)^2+4\omega_A^2\omega_R^2}\,\right].\end{aligned} \tag{19}$$

It appears that the fast (respectively, slow) magnetic Archimedes Coriolis wave propagates faster (respectively, slower) than the fast (slow) magnetic Coriolis wave.

In some previous studies, the inertial term $\partial_t \boldsymbol{u}$, as well as viscous, magnetic and thermal diffusion have been ignored in order to focus on the essential physics involving the Lorentz (magnetic), buoyancy (Archimedes), and Coriolis forces (see Refs [5,12]). In that case, one deduces from system Eq. (10) the following dispersion relation:

$$\omega_R^2\omega^2 - \omega_A^4 - \omega_G^2\omega_A^2 = 0, \tag{20}$$

which is the same as Eq. (5.14) in Ref. [5]. We note that the formulation in terms of the displacement vector of the wave perturbations used by Soward and Dormy [12] [to derive the dispersion relation (20)] clearly shows how magnetic Archimedes Coriolis waves are associated with elliptical motion of fluid particles. Additional properties of the MAC waves can be drawn from the analysis of the phase and group velocities $\boldsymbol{V}_\phi = \omega(k)k^{-2}\boldsymbol{k}$ and $\boldsymbol{V}_g = \boldsymbol{\nabla}_{\boldsymbol{k}}\omega(k)$.

We now briefly examine the similarity between the dispersion relation Eq. (19) and that of f-plane magnetohydrodynamics. Schecter *et al.* [15] analyzed the dynamics of MAC waves in the solar tachocline by using the shallow water magnetohydrodynamics model with the constraint [14],

$$\boldsymbol{\nabla}_h\cdot(\tilde{h}\tilde{\boldsymbol{B}}) = 0, \tag{21}$$

where $\boldsymbol{\nabla}_h = (\partial_{x_1},\partial_{x_2})$ is the horizontal gradient operator and $\tilde{h}(x_1,x_2,t)$ is the instantaneous height of the fluid domain having a horizontally infinite expanse. The latter constraint results from the boundary condition that $\tilde{\boldsymbol{B}}$ is tangent to the free upper surface. They derived a dispersion relation giving the frequencies of unidirectional (along x_1 axis) slow and fast linear MAC modes [see their Eq. (3)], which can be described by Eq. (19), provided

$$\omega_R = f, \quad \omega_G = k_1\sqrt{gH}, \quad \omega_A = \frac{(\boldsymbol{B}\cdot\boldsymbol{e}_1)}{\sqrt{\bar{\varrho}\mu_0}}k_1, \tag{22}$$

where H is the equilibrium thickness of the sublayer of the solar tachocline with average density $\bar{\varrho}$. Using the β-plane approximation, Zaqarashvili *et al.* [16] derived a dispersion relation for two-dimensional magnetic Rossby waves in Cartesian coordinates [see their Eq. (14)], such that, for $\beta = 0$, it transforms into Eq. (19) with

$$\omega_R = f, \quad \omega_G = k_h\sqrt{gH}, \quad \omega_A = \frac{(\boldsymbol{B}\cdot\boldsymbol{e}_1)}{\sqrt{\bar{\varrho}\mu_0}}k_1, \tag{23}$$

where the background magnetic field is along the x_1 direction. Heng and Spitkovsky [17] presented a linear analysis of inviscid, incompressible, MHD shallow water waves in both Cartesian and spherical geometries. In the case of Cartesian coordinates, they considered a vertical basic uniform magnetic

field and derived a dispersion relation [see their Eq. (12)], which can also be described by Eq. (19) with

$$\omega_R = f, \quad \omega_G = k_h\sqrt{gH}, \quad \omega_A = \frac{(\boldsymbol{B}\cdot\boldsymbol{e}_3)}{H\sqrt{\varrho\mu_0}}. \tag{24}$$

The derivation of the MHD shallow water equations [14,15,37] by taking into account the equation for the induction potential scalar $\tilde{\varpi}$ [described by Eq. (3)] would allow us to analyze in more detail the similarity between the dispersion relation Eq. (19) and that of f-plane magnetohydrodynamics. Note that in the shallow water equations the potential vorticity is defined as the absolute vorticity divided by the layer thickness [38].

IV. MAGNETIC CORIOLIS WEAK WAVE TURBULENCE

In this section, we examine the linear processes in initially homogeneous isotropic developed turbulence submitted to both background rotation and a uniform steady magnetic field. From the solution for the poloidal and toroidal kinetic and magnetic modes, we determine the radial spectrum of the kinetic and magnetic energies $S_\kappa(k,t)$ and $S_m(k,t)$. We show that, in the axisymmetric case (i.e., $\boldsymbol{B} \parallel \boldsymbol{\Omega}$), the Alfvén ratio $S_\kappa(k,t)/S_m(k,t)$ behaves like k^{-2} at large scales, in agreement with the recent DNS data by Favier *et al.* [20]. In contrast, in the nonaxisymmetric case (i.e., $\boldsymbol{B} \perp \boldsymbol{\Omega}$), the Alfvén ratio $S_\kappa(k,t)/S_m(k,t)$ behaves like k^{-1}. The analysis of the time development of kinetic and magnetic energies is reported in Appendix B, for the sake of clarity.

Conditions for validity of the linear theory were discussed as follows [36,39,40]. Let ℓ_0 and $u_0(\ell_0)$ be the eddy size and its characteristic velocity where ℓ_0/u_0 represents the eddy overturning time. Assuming that $\|\boldsymbol{u}\| \sim \sqrt{\rho_0\mu_0}\|\boldsymbol{b}\|$. The nonlinear terms $\|(\boldsymbol{u}\cdot\boldsymbol{\nabla})\boldsymbol{u}\|$, $(\rho_0\mu_0)^{-\frac{1}{2}}\|(\boldsymbol{u}\cdot\boldsymbol{\nabla})\boldsymbol{b}\|$ and $(\rho_0\mu_0)^{-1}\|(\boldsymbol{\nabla}\times\boldsymbol{b})\times\boldsymbol{b}\|$ in Eq. (1) are of order $O(u_0^2/\ell_0)$, while the Coriolis term $2\boldsymbol{\Omega}\times\boldsymbol{u}$ is of order $O(fu_0)$. The nonlinear terms involved in the induction equation are $(\rho_0\mu_0)^{-\frac{1}{2}}\|(\boldsymbol{u}\cdot\boldsymbol{\nabla})\boldsymbol{B}\|$ and $(\rho_0\mu_0)^{-1}\|(\boldsymbol{\nabla}\times\boldsymbol{b})\times\boldsymbol{B}\|$, and are of order $O(u_0V_A/\ell_0)$. Therefore, in the case of nonrotating MHD homogeneous turbulence submitted to a uniform magnetic field (i.e., $f=0$, $V_A\neq 0$), the nonlinear terms remain small compared to the Alfvén terms if $u_0 \ll V_A$. This condition characterizes the so-called wave turbulence regime [26]. Obviously, in the so-called strong turbulence limit for which $V_A \approx u_0$, nonlinear interactions play an important role in the turbulence dynamics. For example, the presence of non-Alfvénic fluctuations, which are characterized by an Alfvén ratio of energy (kinetic/magnetic, $E_\kappa(t)/E_m(t)$) slightly smaller than one [20,25–27], is mainly due to nonlinear interactions and cannot be captured by SLT.

Regarding the validity of the LST in rotating MHD turbulence submitted to a uniform magnetic field (i.e., $f \neq 0$, $V_A \neq 0$), both conditions $u_0 \ll V_A$ and $\mathrm{Ro} = u_0/(f\ell_0) \ll 1$ must be satisfied. The latter reflects the fact that nonlinear terms in Eq. (1) are small compared to the Coriolis term $2\boldsymbol{\Omega}\times\boldsymbol{u}$, while the former ($u_0 \ll V_A$) implies that $\mathrm{Ro} \ll \mathcal{L}_h$ where $\mathrm{Ro} = u_0/f\ell_0$ denotes the Rossby number defined as the ratio of the eddy turnover time to the Coriolis parameter and $\mathcal{L}_h = V_A/(f\ell_0)$ denotes the Lehnert number defined as the ratio of the magnetic frequency to the Coriolis one [21,41]. We note that in the DNS study by Favier *et al.* [20]) the Rossby number Ro remains greater than the Lehnert number $\mathcal{L}_h$ (see Table I), while some other LST results are in agreement with DNS data.

TABLE I. Initial values of the parameters for DNS computations used by Favier *et al.* [20].

$\nu=\eta$	ℓ_0	u_0	V_A	f	$\mathrm{Ro}=\frac{u_0}{f\ell_0}$	$\mathcal{L}_h=\frac{V_A}{f\ell_0}$	$\Lambda=\frac{V_A}{f\eta}$
0.0025	0.62	0.78	0.2	32	0.04	0.01	0.5
0.0025	0.62	0.78	0.2	8	0.15	0.04	2.0
0.0025	0.62	0.78	0.2	2	0.60	0.16	8.0

A. Spectral density of energy

Radial spectra, such as $S_\kappa(k)$, which gives kinetic energy per unit mass, $E_\kappa(t) = \int_0^\infty S_\kappa(k,t)dk$, are calculated using

$$S_\kappa(k,t) = k^2\int_0^{2\pi}\int_0^{\pi}\mathcal{E}_\kappa(\boldsymbol{k},t)\sin\theta d\theta d\varphi, \tag{25}$$

where (k,θ,φ) is a spherical coordinate in $\boldsymbol{k}$ space,

$$k_1 = k\cos\varphi\sin\theta, \quad k_2 = k\sin\varphi\sin\theta, \quad k_3 = k\cos\theta, \tag{26}$$

and $\mathcal{E}_\kappa(\boldsymbol{k},t)$ is the spectral density of kinetic energy,

$$\begin{aligned}\mathcal{E}_\kappa(\boldsymbol{k},t) &= \mathcal{E}_\kappa^{(1)}(\boldsymbol{k},t) + \mathcal{E}_\kappa^{(2)}(\boldsymbol{k},t),\\ \mathcal{E}_\kappa^{(1)}(\boldsymbol{k},t) &= \tfrac{1}{2}\langle|u^{(1)}|^2\rangle, \quad \mathcal{E}_\kappa^{(2)}(\boldsymbol{k},t) = \tfrac{1}{2}\langle|u^{(2)}|^2\rangle,\end{aligned} \tag{27}$$

where $\mathcal{E}_\kappa^{(1)}$ and $\mathcal{E}_\kappa^{(2)}$ are the toroidal and poloidal spectral densities of kinetic energy, respectively, and $\langle\ \cdot\ \rangle$ denotes ensemble (statistical) averaging. The spectral density of vertical kinetic energy is related to $\mathcal{E}_\kappa^{(2)}$ as

$$\mathcal{E}_\kappa^{(v)}(\boldsymbol{k},t) = \tfrac{1}{2}\langle|\hat{u}_3|^2\rangle = \sin^2\theta\ \mathcal{E}_\kappa^{(2)}(\boldsymbol{k},t), \tag{28}$$

while

$$\begin{aligned}\mathcal{E}_\kappa^{(h)}(\boldsymbol{k},t) &= \tfrac{1}{4}(\langle|\hat{u}_1|^2\rangle + \langle|\hat{u}_2|^2\rangle)\\ &= \tfrac{1}{2}\big(\mathcal{E}_\kappa(\boldsymbol{k},t) - \mathcal{E}_\kappa^{(v)}(\boldsymbol{k},t)\big)\end{aligned} \tag{29}$$

represents the spectral density of horizontal kinetic energy. Likewise, we define the spectral density of magnetic energy (per unit mass) components,

$$\mathcal{E}_m = \mathcal{E}_m^{(1)} + \mathcal{E}_m^{(2)} = \mathcal{E}_m^{(v)} + 2\mathcal{E}_m^{(h)}.$$

Recall that, in the linear inviscid limit, the total (kinetic+magnetic) energy is conserved, so that

$$\mathcal{E}_\kappa(\boldsymbol{k},t) + \mathcal{E}_m(\boldsymbol{k},t) = \mathcal{E}_\kappa(\boldsymbol{k},0) + \mathcal{E}_m(\boldsymbol{k},0), \tag{30}$$

and energy exchange between magnetic and kinetic components is ensured by the cross-correlation between the velocity and the magnetic field fluctuations,

$$\dot{\mathcal{E}}_\kappa = -\mathcal{F}_{\kappa m}, \quad \dot{\mathcal{E}}_m = \mathcal{F}_{\kappa m}, \tag{31}$$

where

$$\mathcal{F}_{\kappa m} = -\omega_A\langle\Re(\mathrm{i}\hat{u}_j\hat{b}_j^*)\rangle = \omega_A\langle\Re(u^{(1)}u^{(3)*} + u^{(2)}u^{(4)*})\rangle$$

is the spectral density of the cross-correlation, and the superscript * denotes complex conjugate.

Since the turbulence is initially nearly isotropic in usual laboratory experiments on grid turbulence (see, e.g., Ref. [42]) and in DNS, we consider, in this study, initially isotropic turbulence with vanishing initial magnetic energy, so that

$$\begin{aligned}\langle u_0^{(1)}u_0^{(1)*}\rangle &= \langle u_0^{(2)}u_0^{(2)*}\rangle = \frac{S(k,0)}{4\pi k^2},\\ \langle \mathrm{Re}(u_0^{(1)}u_0^{(2)*})\rangle &= \langle \mathrm{Re}(u_0^{(3)}u_0^{(4)*})\rangle = 0,\\ \langle u_0^{(3)}u_0^{(3)*}\rangle &= \langle u_0^{(4)}u_0^{(4)*}\rangle = 0,\end{aligned} \tag{32}$$

where $S_\kappa(k,0)$ is the initial energy spectrum. We further assume that the cross-correlation is initially zero: $\langle \mathrm{Re}(u_0^{(\alpha)}u_0^{(\beta)*})\rangle = 0$ with $\alpha = 1,2$ and $\beta = 3,4$.

From the solution of system Eq. (10) reported in Appendix A 1, we determine the spectral density of kinetic and magnetic energies, and the cross-correlation (for a diffusionless fluid),

$$\begin{aligned}\mathcal{E}_\kappa^{(1)} = \mathcal{E}_\kappa^{(2)} &= \frac{S(k,0)}{8\pi k^2}\left[\frac{(\omega_R^2+2\omega_A^2)}{(\omega_R^2+4\omega_A^2)}\right.\\ &\left.+\frac{2\omega_A^2}{(\omega_R^2+4\omega_A^2)}\cos\left(t\sqrt{\omega_R^2+4\omega_A^2}\right)\right],\\ \mathcal{E}_m^{(1)} = \mathcal{E}_m^{(2)} &= \frac{S(k,0)}{8\pi k^2}\left[\frac{2\omega_A^2}{(\omega_R^2+4\omega_A^2)}\right.\\ &\left.-\frac{2\omega_A^2}{(\omega_R^2+4\omega_A^2)}\cos\left(t\sqrt{\omega_R^2+4\omega_A^2}\right)\right],\end{aligned} \tag{33}$$

$$\begin{aligned}\mathcal{F}_{\kappa m} &= \frac{\partial \mathcal{E}_m}{\partial t} = -\frac{\partial \mathcal{E}_\kappa}{\partial t}\\ &= \frac{S(k,0)}{4\pi k^2}\left[\frac{2\omega_A^2}{\sqrt{(\omega_R^2+4\omega_A^2)}}\sin\left(t\sqrt{\omega_R^2+4\omega_A^2}\right)\right].\end{aligned} \tag{34}$$

As expected, there is equipartition of energy between poloidal and toroidal components, but not between horizontal and vertical components,

$$\begin{aligned}\left(\mathcal{E}_\kappa^{(v)},\mathcal{E}_m^{(v)}\right) &= \sin^2\theta\left(\mathcal{E}_\kappa^{(2)},\mathcal{E}_m^{(2)}\right),\\ \left(\mathcal{E}_\kappa^{(h)},\mathcal{E}_m^{(h)}\right) &= \tfrac{1}{2}(2-\sin^2\theta)\left(\mathcal{E}_\kappa^{(2)},\mathcal{E}_m^{(2)}\right),\end{aligned} \tag{35}$$

and the unsteady part of the spectral densities exhibit an oscillatory behavior with period $T = 2\pi/(\omega_f+\omega_s) = 2\pi/(\sqrt{\omega_R^2+4\omega_A^2})$. Recall that $\omega_A = \boldsymbol{V}_a\cdot\boldsymbol{k} = V_a k_3$ and $\omega_R = fk_3/k$.

As indicated previously, in the case of nonzero viscosity and diffusion, the solutions generally become much more complicated because of oscillations due to differential diffusion, but if $\nu = \eta$, the solution takes a much simpler form, so that one needs to multiply the spectral density of energies obtained in the inviscid case by the factor $\mathrm{e}^{-2\nu k^2 t}$.

B. Spectra

When the magnetic field aligns with the rotation axis ($\boldsymbol{B} \parallel \boldsymbol{\Omega}$), the Alfvén and Coriolis frequencies do not depend on the azimuthal angle φ (axisymmetric case),

$$\omega_A = V_a k\cos\theta, \quad \omega_R = f\cos\theta.$$

We substitute these forms into Eq. (33) and integrate with respect to the polar angle θ, we then obtain the radial spectrum of kinetic and magnetic energies, and the cross-correlation for a diffusive fluid with $P_{\mathrm{rm}} = P_{\mathrm{rt}} = 1$,

$$\begin{aligned}S_\kappa(k,t) &= S_\kappa(k,0)\left[\frac{D_1}{D_0}+\frac{D_2}{D_0}\frac{\sin(t\sqrt{D_0})}{t\sqrt{D_0}}\right]e^{-2\nu k^2 t},\\ S_m(k,t) &= S_\kappa(k,0)\left[1-\frac{D_1}{D_0}-\frac{D_2}{D_0}\frac{\sin(t\sqrt{D_0})}{t\sqrt{D_0}}\right]e^{-2\nu k^2 t},\\ F_{\kappa m}(k,t) &= \dot{S}_m(k,t)+2\nu k^2 S_m(k,t)\\ &= \frac{S_\kappa(k,0)}{t}\frac{D_2}{D_0}\left[\frac{\sin(t\sqrt{D_0})}{t\sqrt{D_0}}-\cos(t\sqrt{D_0})\right]e^{-2\nu k^2 t},\end{aligned} \tag{36}$$

where

$$\begin{aligned}D_0(k) &= f^2+4(V_A k)^2,\\ D_1(k) &= f^2+2(V_A k)^2,\\ D_2(k) &= 2(V_A k)^2.\end{aligned} \tag{37}$$

Theoretical insight can be gained in understanding effects of linear processes on the energy partition, scale by scale, by analyzing the behavior of the spectral Alfvén ratio $S_\kappa(k,t)/S_m(k,t)$, which becomes exactly identical to the inviscid ratio,

$$\frac{S_\kappa(k,t)}{S_m(k,t)} = \frac{\frac{D_1}{D_0}+\frac{D_2}{D_0}\frac{\sin(t\sqrt{D_0})}{t\sqrt{D_0}}}{1-\frac{D_1}{D_0}-\frac{D_2}{D_0}\frac{\sin(t\sqrt{D_0})}{t\sqrt{D_0}}}.$$

At sufficiently short times such as $t\sqrt{D_0} \ll 1$, the Alfvén ratio $S_\kappa(k,t)/S_m(k,t)$ behaves like $(V_A k)^{-2}t^{-2}$. At large dimensionless time $ft \gg 1$, the contribution of the unsteady part of the spectrum becomes negligible and the ratio $S_\kappa(k,t)/S_m(k,t)$ approaches the limit,

$$\lim_{ft\to\infty}\frac{S_\kappa(k,t)}{S_m(k,t)} = \frac{D_1}{D_0-D_1} = \frac{1+2\mathcal{L}_k^2}{2\mathcal{L}_k^2}, \tag{38}$$

in which $\mathcal{L}_k$ denotes the scale-dependent Lehnert number [41],

$$\mathcal{L}_k = \frac{V_a k}{f}. \tag{39}$$

Therefore, at large scales ($V_a k/f \ll 1$), the local Alfvén ratio S_κ/S_m behaves like $(f^2/V_A^2)k^{-2}$, whereas at small scales ($k\ell_0 \gg 1$) it approaches unity, showing equipartition of energy between kinetic and magnetic components. We note that, in absence of rotation $f = 0$, the long-time limit of the ratio $S_\kappa(k,t)/S_m(k,t)$ is unity for all scales. Therefore, we may conclude that, at large scales, rotation prevents the occurrence of equipartition between kinetic and magnetic energies as illustrated by Fig. 1 displaying the variation of the Alfvén ratio $S_\kappa(k,t)/S_m(k,t)$ in function of $\mathcal{L}_k = V_A k/f$. We also report in Fig. 1 the DNS data collected from Fig. 9 in Favier *et al.* [20], displaying the radial spectrum of kinetic and magnetic energies at the dimensionless time $t^+ = (u_0/\ell_0)t = 5$ and several values of the Elsasser number $\Lambda = V_A/(f\eta)$ (see Table I). In these numerical simulations, the initial Taylor microscale Reynolds number is about $\mathrm{Re}_\lambda = 72$.

As can be expected, at $V_A k/f < 1$, there is agreement between LST results and DNS data. This signifies that the

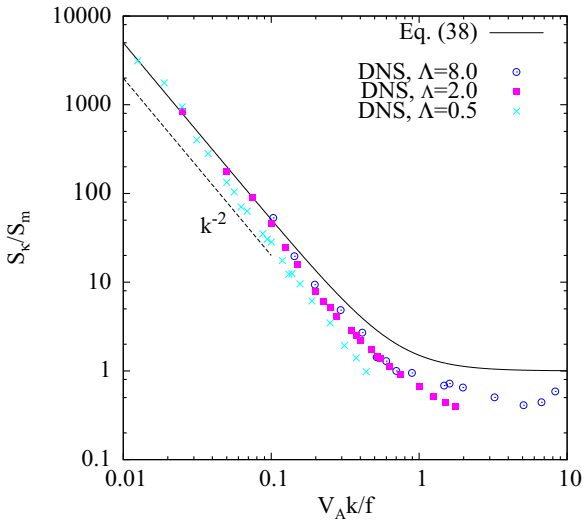

FIG. 1. Variation of the Alfvén ratio, $S_\kappa(k,t)/S_m(k,t)$, in function of the scale-dependent Lehnert number $\mathcal{L}_k = V_A k/f$ in a rotating homogeneous turbulence submitted to a uniform magnetic field aligning with the rotation axis (axisymmetric case). The figure compares the LST results given by Eq. (38) and the DNS data collected from Fig. 9 in Ref. [20] displaying the radial spectrum of kinetic and magnetic energies obtained at $t^+ = (u_0/\ell_0)t = \mathrm{Ro}(ft) = 5$ and three values of the Elsasser number $\Lambda = 0.5$, 2.0, 8.0 (see Table I). The figure shows that, at $V_A k/f < 1$, LST is in agreement with DNS. At $V_A k/f > 1$, LST predicts an equipartition of energy between magnetic and kinetic components while DNS data indicate that the Alfvén ratio is smaller than one characterizing a non-Alfvénic regime.

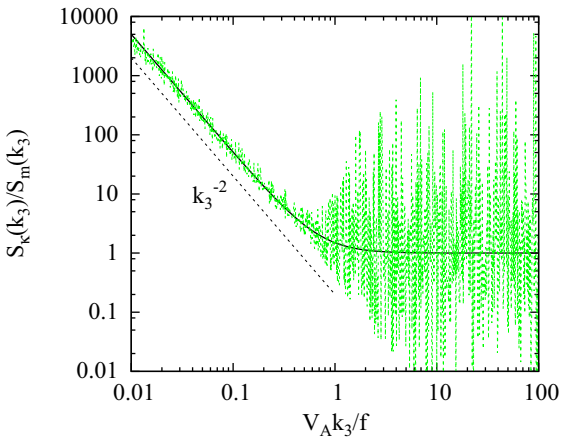

FIG. 2. Variation of the Alfvén ratio, $S_\kappa(k_3,t)/S_m(k_3,t)$, in function of the vertical scale-dependent Lehnert number $V_A k_3/f$ at $ft = 100$ in a rotating homogeneous turbulence submitted to a uniform magnetic field aligning with the rotation axis (axisymmetric case). The green curve represents the numerical results for the ratio $S_\kappa(k_3,t)/S_m(k_3,t)$. These one-dimensional spectra in the vertical direction have been determined numerically by integrating the spectral density of energy for a diffusive fluid with $P_{\mathrm{rm}} = \nu/\eta = 1$ and $P_{\mathrm{rt}} = \nu/\kappa = 1$ using the initial spectrum $S_\kappa(k,0) \propto k^2 \mathrm{e}^{-k_0^{-2}k^2}$ [see Eq. (61)]. As expected, the numerical results fluctuate around the black curve $[1 + (2V_A^2 k_3^2 f^{-2})^{-1}]$ (details on the derivation of the above expression are reported in Appendix C). It is clear that, at large vertical scales ($V_A k_3/f \ll 1$), the Alfvén ratio behaves like k_3^{-2} and, at small scales ($V_A k_3/f \gg 1$), there is an equipartition of energy.

transfer of energy from the kinetic fluctuations to the magnetic ones, which occurs at large scales, is mainly due to linear processes. Recall that the initial magnetic energy is assumed to be zero (as in the DNS study by Ref. [20]). For $V_A k/f > 1$, DNS data show that the Alfvén ratio is smaller than one characterizing a non-Alfvénic regime induced by the nonlinear interactions. This behavior cannot be captured by LST, which predicts an equipartition of energy between magnetic and kinetic components.

We note that, when the initial magnetic energy is not zero, the long-time limit of the local Alfvén ratio takes the form

$$\lim_{ft\to\infty} \frac{S_\kappa(k,t)}{S_m(k,t)} = \frac{1 + 2[1+\xi(k)]\mathcal{L}_k^2}{\xi(k) + 2[1+\xi(k)]\mathcal{L}_k^2}, \tag{40}$$

where $\xi(k) = S_m(k,0)/S_\kappa(k,0)$. According to the recent study of nonhelical inverse transfer of a decaying turbulent magnetic field by Brandenburg *et al.* [43], there is a k^2 subinertial range spectrum of kinetic energy forcing the magnetic field with a k^4 subinertial range to attain larger-scale coherence, so that $\xi(k) \propto k^2$ at these large scales. The substitution of this form into Eq. (40) yields $S_\kappa(k,t)/S_m(k,t) \propto k^{-2}$ (at large scales).

Also, the analysis of the one-dimensional spectrum in the vertical (x_3) direction, which is parallel to the uniform magnetic field $\boldsymbol{B}$,

$$\mathcal{S}_\kappa(k_3,t) = \iint_{-\infty}^{+\infty} \mathcal{E}_\kappa(\boldsymbol{k},t)\,dk_1 dk_2,$$

shows that at large vertical scales ($V_A k_3/f \ll 1$) the ratio $\mathcal{S}_\kappa(k_3,t)/\mathcal{S}_m(k_3,t)$ behaves like $[1 + (2V_A^2 k_3^2/f^2)^{-1}]$ for long times (see Appendix C) as illustrated by Fig. 2. Therefore, at large scales ($V_A k_3/f \ll 1$) it behaves like $k_3^{-2} \equiv k_\parallel^{-2}$, and at small scales ($V_A k_3/f \gg 1$) there is equipartition of energy.

To end this section, we briefly address the case where the magnetic field is perpendicular to rotation axis (i.e., asymmetric case), it being the most plausible configuration inside the Earth's core [23,24]. In that case, the competition between Alfvén and inertial waves is more complex, depending not only on the scale and on the polar angle θ between $\boldsymbol{k}$ and $\boldsymbol{\Omega}$ but also on the azimuthal angle φ between $\boldsymbol{k}$ and $\boldsymbol{V}_A$,

$$\omega_A = V_A k_1 = V_A k \sin\theta\cos\varphi, \quad \omega_R = f\cos\theta.$$

We show that the unsteady part of $S_\kappa(k,t)$ and $S_m(k,t)$ approaches zero for long times and the local Alfvén ratio $S_\kappa(k,t)/S_m(k,t)$ approaches its long-time limit (see Appendix D),

$$\lim_{t\to\infty} \frac{S_\kappa(k,t)}{S_m(k,t)} = \frac{f + 2(V_A k)}{2(V_A k)} = \frac{1 + 2\mathcal{L}_k}{2\mathcal{L}_k}. \tag{41}$$

The latter equation indicates that at large scales (i.e., $V_A k/f \ll 1$) the Alfvén ratio behaves like k^{-1}, whereas at small scales (i.e., $V_A k/f \gg 1$) there is equipartition of energy between

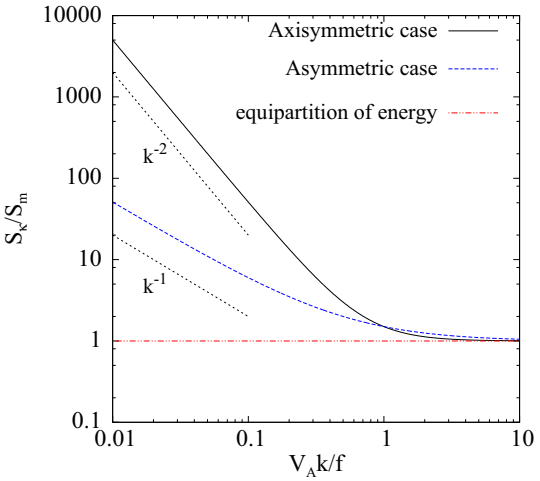

FIG. 3. Variation of the Alfvén ratio, $S_\kappa(k,t)/S_m(k,t)$, in function of the scale-dependent Lehnert number $\mathcal{L}_k = V_A k/f$ in a rotating homogeneous turbulence submitted to a uniform magnetic field which is either parallel (axisymmetric case) or perpendicular (asymmetric case) to the rotation axis. The figure illustrates the fact that, in the axisymmetric case, the inertial waves affect more the dynamics of large scales (induced by the Alfvén waves in the absence of rotation) than in the asymmetric case, but in both cases the equipartition of energy is broken.

kinetic and magnetic components as in the axisymmetric case (see Fig. 3 as an illustration).

C. Comments about dissipation and horizontal and vertical anisotropy

In homogeneous turbulence, the kinetic dissipation rate ε_κ and the magnetic dissipation rate ε_m per unit mass can be defined as [44]

$$\varepsilon_\kappa = \nu\langle\|\nabla\times\boldsymbol{u}\|^2\rangle = 2\nu\int_0^\infty k^2 S_\kappa(k,t)dk,$$
$$\varepsilon_m = \frac{\eta}{\rho_0\mu_0}\langle\|\nabla\times\boldsymbol{b}\|^2\rangle = 2\eta\int_0^\infty k^2 S_m(k,t)dk. \tag{42}$$

Therefore, scale by scale, the ratio of the kinetic dissipation rate to the magnetic dissipation rate behaves like the Alfvén ratio $S_\kappa(k,t)/S_m(k,t)$. At large scales, it behaves like k^{-2} and remains greater than one, while at small scales, viscous and Joule dissipations are equal.

Although SLT reproduces correctly the distribution of energy between magnetic and kinetic components, it incorrectly predicts the anisotropy of magnetic and velocity fluctuations as we briefly discuss now. The radial spectrum of the vertical kinetic and magnetic energies can be determined in a similar manner,

$$S_\kappa^{(v)}(k,t) = \frac{S_\kappa(k,0)}{3}\left[\frac{D_1}{D_0} - \frac{D_2}{D_0}\left(\frac{\cos(t\sqrt{D_0})}{t^2 D_0} - \frac{\sin(t\sqrt{D_0})}{t^3 D_0^{\frac{3}{2}}}\right)\right]e^{-2\nu k^2 t},$$

$$S_m^{(v)}(k,t) = \frac{S_\kappa(k,0)}{3}\left[1 - \frac{D_1}{D_0} + \frac{D_2}{D_0}\left(\frac{\cos(t\sqrt{D_0})}{t^2 D_0} - \frac{\sin(t\sqrt{D_0})}{t^3 D_0^{\frac{3}{2}}}\right)\right]e^{-2\nu k^2 t}, \tag{43}$$

while the radial spectrum of the horizontal components can be obtained using

$$S_\kappa^{(h)}(k,t) = \tfrac{1}{2}\big(S_\kappa(k,t) - S_\kappa^{(v)}(k,t)\big),$$
$$S_m^{(h)}(k,t) = \tfrac{1}{2}\big(S_m(k,t) - S_m^{(v)}(k,t)\big). \tag{44}$$

Therefore, the ratios $S_\kappa^{(h)}/S_\kappa^{(v)}$ and $S_m^{(h)}/S_m^{(v)}$ characterizing the anisotropy of the velocity and magnetic fluctuations approach unity at all scales for long times. The recent DNS data by Favier *et al.* [20] show that, in the nonrotating MHD case (i.e., $f = 0$, $V_A \neq 0$), these two ratios are about unity at all scales. In counterpart, in rotating homogeneous turbulence submitted to a magnetic field (i.e., $f \neq 0$, $V_A \neq 0$), vertical kinetic energy is dominant ($S_\kappa^{(h)}/S_\kappa^{(v)} < 1$), whereas horizontal magnetic energy is dominant ($S_m^{(h)}/S_m^{(v)} > 1$; see Fig. 12 in Ref. [20]). The inability of SLT to capture this anisotropy is due to the fact that for initial isotropic conditions the diagonal component in the vertical direction π_{33} of the linear pressure-strain correlation is zero and hence vertical kinetic energy is not affected by rotation since there is no redistribution of energy between the vertical and horizontal motions [40], which occurs only from nonlinear interactions for this flow configuration.

V. MAGNETIC ARCHIMEDES CORIOLIS WEAK WAVE TURBULENCE

In this section, we consider rotating stably stratified homogeneous turbulence submitted to a uniform magnetic field that aligns with the rotation axis and the background density gradient. As in Sec. IV, we consider initial isotropic conditions [see Eq. (32)], assuming that initial magnetic and potential energies are zero. We also assume that the cross-correlation between velocity and magnetic (or density) field fluctuations are initially zero. For the sake of simplicity, we only address the case where $\nu = \eta = \kappa$, and we focus on the energy partition, scale by scale, between magnetic, kinetic, and potential components.

We begin our analysis by considering the case without rotation (i.e., MA wave turbulence). In that case, the spectral density of kinetic ($\mathcal{E}_\kappa$), magnetic ($\mathcal{E}_m$), and potential ($\mathcal{E}_p$) modes deduced from Eqs. (A6) and (A7) are found as

$$\mathcal{E}_\kappa(\boldsymbol{k},t) = \frac{S_\kappa(k,0)}{8\pi k^2}[\cos^2(\omega_A t) + \cos^2(\omega_{AG} t)]e^{-2\nu k^2 t},$$
$$\mathcal{E}_m(\boldsymbol{k},t) = \frac{S_\kappa(k,0)}{8\pi k^2}\left[\sin^2(\omega_A t) + \frac{\omega_A^2}{\omega_{AG}^2}\sin^2(\omega_{AG} t)\right]e^{-2\nu k^2 t},$$
$$\mathcal{E}_p(\boldsymbol{k},t) = \frac{S_\kappa(k,0)}{8\pi k^2}\left[\frac{\omega_G^2}{\omega_{AG}^2}\sin^2(\omega_{AG} t)\right]e^{-2\nu k^2 t}, \tag{45}$$

where the frequencies ω_A, ω_G, and ω_{AG} given by Eqs. (9) and (11) are recalled:

$$\omega_A = V_A k\cos\theta, \quad \omega_G = N\sin\theta, \\ \omega_{AG} = \sqrt{V_A^2 k^2\cos^2\theta + N^2\sin^2\theta}. \tag{46}$$

Because the mean density gradient aligns with the uniform magnetic field (axisymmetric case), the frequencies are independent of the azimuthal angle φ. For a diffusionless fluid, the spectral density of total (kinetic+magnetic+potential) energy is time-independent,

$$\mathcal{E}_\kappa(\boldsymbol{k},t) + \mathcal{E}_m(\boldsymbol{k},t) + \mathcal{E}_p(\boldsymbol{k},t) = \frac{S_\kappa(k,0)}{4\pi k^2},$$

while for a diffusive fluid with $\nu = \eta = \kappa$, it decays with time in an exponential manner due to the diffusion coefficient,

$$\mathcal{E}_\kappa(\boldsymbol{k},t) + \mathcal{E}_m(\boldsymbol{k},t) + \mathcal{E}_p(\boldsymbol{k},t) = \frac{S_\kappa(k,0)}{4\pi k^2}\mathrm{e}^{-2\nu k^2 t}.$$

The integration over the polar angle $0 \leqslant \theta \leqslant \pi$ of the spectral density of energy yields the expression of the radial spectrum, for instance,

$$\frac{S_\kappa(k,t)}{S_\kappa(k,0)} = \left\{\frac{1}{2} + \frac{1}{8}[I_1(k) + I_2(k)]\right\}\mathrm{e}^{-2\nu k^2 t}, \\ I_1(k) = \int_0^\pi \cos(2tV_A k\cos\theta)\sin\theta\, d\theta, \\ I_2(k) = \int_0^\pi \cos\left(2t\sqrt{V_A^2 k^2\cos^2\theta + N^2\sin^2\theta}\right)\sin\theta\, d\theta. \tag{47}$$

Except at $V_A k = N$, it is not simple to compute analytically the integral $I_2(k)$. For this, we use the method of stationary phase (or equivalently, the method of steepest descent [45]) to evaluate it (see below).

When $V_A k = N$, the dispersion relation for the magnetic gravity wave reduces to $\omega_{AG} = V_A k = N$ with a nonzero value for the group velocity of the wave, $\boldsymbol{V}_g(k = N/V_A) = V_A\boldsymbol{e}_3$. It is interesting to note that in the case of inertia-gravity waves, the dispersion relation is of the form $\omega_{\mathrm{IG}} = \sqrt{f^2\cos^2\theta + N^2\sin^2\theta}$, and when $f = N$, it reduces to $\omega_{\mathrm{IG}} = f = N$ with a zero value for the group velocity signifying that the wave energy does not propagate [36].

In the case where $V_A k = N$, the radial spectrum takes the form

$$\frac{S_\kappa(k,t)}{S_\kappa(k,0)} = \left\{\frac{1}{2} + \frac{1}{4}\left[\cos(2Nt) + \frac{\sin(2Nt)}{2Nt}\right]\right\}e^{-2\nu k^2 t}, \\ \frac{S_m(k,t)}{S_\kappa(k,0)} = \left\{\frac{1}{3} - \frac{1}{4}\left[\frac{1}{3}\cos(2Nt) + \frac{\sin(2Nt)}{2Nt}\right]\right\}e^{-2\nu k^2 t}, \\ \frac{S_p(k,t)}{S_\kappa(k,0)} = \frac{1}{6}[1 - \cos(2Nt)]e^{-2\nu k^2 t}. \tag{48}$$

Therefore, at large dimensionless time $Nt \gg 1$, the contribution of the term $\sin(2Nt)/(2Nt)$ is not significant and the ratio $S_p(N/V_A,t)/S_\kappa(N/V_A,t)$ (respectively, $S_p(N/V_A,t)/S_m(N/V_A,t)$) oscillates between 0 and 4/3 (respectively, 0 and 4/5).

When $V_A k \neq N$ and

$$\max\left(t\nu k^2, t\sqrt{V_A^2 k^2 + N^2}\right) \ll 1,$$

we determine the short-time approximations of the radial spectrum,

$$\frac{S_\kappa(k,t)}{S_\kappa(k,0)} = 1 - 2\nu k^2 t - \frac{1}{3}\left(V_A^2 k^2 + N^2\right)t^2 + \ldots, \\ \frac{S_m(k,t)}{S_\kappa(k,0)} = \frac{1}{3}V_A^2 k^2 t^2 + \ldots, \\ \frac{S_p(k,t)}{S_\kappa(k,0)} = \frac{1}{3}N^2 t^2 + \ldots, \tag{49}$$

where ... indicate high-order terms. It appears that, at large scales ($V_A k/N \ll 1$) and to order $O[(Nt)^3]$, the potential energy is independent of the radial wave number k and remains more important than the magnetic energy, while the dominant corrective term in the development of the kinetic energy is due to viscosity.

To derive the long-time approximations of the radial spectrum when $V_A k \neq N$, we use the method of stationary phase to estimate the integral $I_2(k)$, as already indicated. In fact, the components that satisfy $\partial\omega_{AG}/\partial\theta = 0$ are the most slowly oscillating components with θ in the integrand and contribute most to the integral. Note that this method has been applied for stratified and rotating homogeneous turbulence [36,46] and gives good approximations even when the time is not very large [45]. Because the stationary phase $\theta_0 = \pi/2$ satisfies $\cos\theta_0 = 0$, so that $\omega_{AG}(\theta_0) = N$, the Lorentz force effects (through the Alfvén frequency) in the integrand cannot contribute significantly to the integral in the long-time limit. The result is

$$\frac{S_\kappa(k,t)}{S_\kappa(k,0)} = \left\{\frac{1}{2} + \frac{1}{4}\left[\frac{\sin(2\mathcal{L}_g Nt)}{2\mathcal{L}_g Nt} + \sqrt{\frac{\pi}{|\mathcal{L}_g^2 - 1|}}\frac{\cos\left(2Nt \pm \frac{\pi}{4}\right)}{2\sqrt{Nt}}\right]\right\}e^{-2\nu k^2 t}, \\ \frac{S_m(k,t)}{S_\kappa(k,0)} = \left(\frac{1}{2} - \frac{1}{4}\left\{h(\mathcal{L}_g) + \frac{\sin(2\mathcal{L}_g Nt)}{2\mathcal{L}_g Nt} + \sqrt{\frac{\pi}{|\mathcal{L}_g^2 - 1|}}\left[\frac{\cos\left(2Nt \pm \frac{\pi}{4}\right)}{2\sqrt{Nt}} - \frac{\sin\left(2Nt \pm \frac{\pi}{4}\right)}{\sqrt{Nt}}\right]\right\}\right)e^{-2\nu k^2 t}, \\ \frac{S_p(k,t)}{S_\kappa(k,0)} = \frac{1}{4}\left[h(\mathcal{L}_g) - \sqrt{\frac{\pi}{|\mathcal{L}_g^2 - 1|}}\frac{\sin\left(2Nt \pm \frac{\pi}{4}\right)}{\sqrt{Nt}}\right]e^{-2\nu k^2 t}, \tag{50}$$

where $\mathcal{L}_g = V_a k/N$ denotes the ratio of the maximal Alfvén frequency to the maximal gravity frequency and

$$h(\mathcal{L}_g) = \frac{\mathcal{L}_g^2}{\left(\mathcal{L}_g^2-1\right)^{\frac{3}{2}}}\tan^{-1}\left(\sqrt{\mathcal{L}_g^2-1}\right) - \frac{1}{\mathcal{L}_g^2-1} \quad \text{if} \quad \mathcal{L}_g > 1,$$
$$h(\mathcal{L}_g) = \frac{\mathcal{L}_g^2}{\left(1-\mathcal{L}_g^2\right)^{\frac{3}{2}}}\log\left(\frac{1-\sqrt{1-\mathcal{L}_g^2}}{1+\sqrt{1-\mathcal{L}_g^2}}\right) + \frac{1}{1-\mathcal{L}_g^2} \quad \text{if} \quad \mathcal{L}_g < 1. \tag{51}$$

Accordingly, one can deduce the long-time limit of the ratios

$$\lim_{Nt\to\infty}\frac{S_p(k,t)}{S_\kappa(k,t)} = \frac{h(\mathcal{L}_g)}{2}, \quad \lim_{Nt\to\infty}\frac{S_p(k,t)}{S_m(k,t)} = \frac{h(\mathcal{L}_g)}{2-h(\mathcal{L}_g)}. \tag{52}$$

At large scales ($\mathcal{L}_g = V_A k/N \ll 1$), one has $h(\mathcal{L}_g) \sim 1$, and hence the ratio $S_p(k,t)/S_m(k,t)$ approaches one signifying that there is equipartition of energy between magnetic and potential components independently of the form of the initial spectrum $S_\kappa(k,0)$, while the Alfvén ratio $S_\kappa(k,t)/S_m(k,t)$ approaches 2, for long times.

At small scales, $\mathcal{L}_g = V_A k/N \gg 1$, the function $h(\mathcal{L}_g)$ behaves like $\mathcal{L}_g^{-1}$. Therefore, the Alfvén ratio $S_\kappa(k,t)/S_m(k,t)$ approaches one indicating an equipartition of energy between the magnetic and kinetic components, as in the case of MC weak wave turbulence, whereas the ratios $S_p(k,t)/S_\kappa(k,t)$ and $S_p(k,t)/S_m(k,t)$ behave like k^{-1} (see the top panel in Fig. 4 as an illustration).

It should be noted that, in the case of a diffusionless fluid, the kinetic energy approaches $\frac{1}{2}S_\kappa(k,0)$ at all scales (see the bottom panel in Fig. 4). In counterpart, the potential energy approaches $\frac{1}{4}S_0(k,0)$ at large scales and zero at small scales. Recall that the energy ratio, scale by scale, is the same

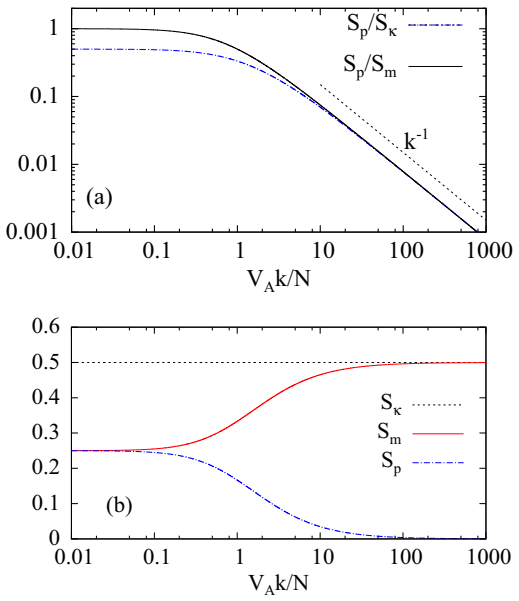

FIG. 4. Case of magnetic Archimedes wave weak turbulence. Panel (a) shows, scale by scale, the long-time behavior of the energy ratios potential/kinetic and potential/magnetic. It indicates that, at large scales ($V_A k/N \ll 1$), these ratio exhibit a k^0 form and there is an equipartition of energy between magnetic and potential components. At small scales ($V_A k/N \gg 1$), these energy ratios potential/kinetic and potential/magnetic behave like k^{-1}. At small scales, the gravity waves do not alter the equipartition of energy between kinetic and magnetic components induced by the linear dynamic of the Alfvén waves. Panel (b) displays the long-time behavior of the radial spectrum of kinetic, magnetic, and potential energies normalized by the initial spectrum $S_\kappa(k,0)$ for a diffusionless fluid. It indicates that, at small scales, the potential energy approaches zero, while both the kinetic and magnetic components approach $\frac{1}{2}S_\kappa(k,0)$. The kinetic energy is the same ($= \frac{1}{2}S_\kappa(k,0)$) at all scales.

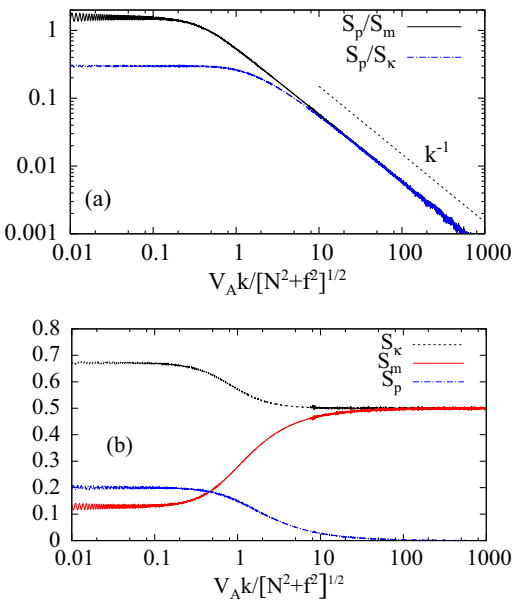

FIG. 5. Case of magnetic Archimedes Coriolis wave turbulence. Panel (a) shows, scale by scale, the long-time behavior of the energy ratios potential/kinetic and potential/magnetic. It indicates that, at large scales ($V_A k/\sqrt{f^2+N^2} \ll 1$), these ratio exhibit a k^0 form, while at small scales ($V_A k/\sqrt{f^2+N^2} \gg 1$), they behave like k^{-1} as in the magnetic Archimedes weak wave turbulence. At small scales, neither the gravity waves nor the inertial waves alter the equipartition of energy between kinetic and magnetic components induced by the linear dynamic of the Alfvén waves. Panel (b) displays the the long-time behavior of the radial spectrum normalized by the initial spectrum $S_\kappa(k,0)$ at large times for a diffusionless fluid. It indicates that, at small scales, the potential energy approaches zero, while both the kinetic and magnetic components approach $\frac{1}{2}S_\kappa(k,0)$.

considering either a diffusionless fluid or a diffusive fluid with $\nu = \eta = \kappa$ and remains independent of the form of the initial spectrum $S(k,0)$.

In the case of magnetic-inertia gravity waves, there are slow and fast waves with frequency ω_S and ω_F described by Eq. (19), as indicated previously Sec. III. In that case, radial spectra are computed numerically by integrating the spectral density of energy deduced from the analytical solution for the Fourier modes [see Eq. (A8)]. Our findings, in this case, can be summarized as follows.

At small scales ($V_A k/\sqrt{f^2+N^2} \gg 1$), there is equipartition of energy between kinetic and magnetic components (see Fig. 5), as for the cases of MC weak wave turbulence and MA wave turbulence. At these small scales, the energy ratios $S_p(k,t)/S_m(k,t)$ and $S_p(k,t)/S_\kappa(k,t)$ behave like k^{-1} for long times as in the case of MA weak wave turbulence.

A consequence of rotation acting at large scales ($V_A k/\sqrt{f^2+N^2} \ll 1$) is that the long-time limit of $S_p(k,t)/S_m(k,t)$ is $\frac{3}{2}$, while in the case of MA weak wave turbulence it is unity. More details on rotation effects can be drawn by considering a diffusionless fluid. In that case, the bottom panel in Fig. 5 reveals that, at large scales, both kinetic and potential energies increase, with respect to the case without rotation, so that the magnetic energy decreases since the total (kinetic+potential+magnetic) energy is conserved in the linear inviscid limit. The long-time limit of $S_p(k,t)$, $S_\kappa(k,t)$, and $S_m(k,t)$ is $\frac{1}{5}S_\kappa(k,0)$, $\frac{2}{3}S_\kappa(k,0)$, and $\frac{2}{15}S_\kappa(k,0)$, respectively. At intermediate scales, the kinetic and potential energies decrease, whereas the magnetic energy increases (see the bottom panel in Fig. 5).

VI. CONCLUDING REMARKS

We have analyzed in detail the effects of linear processes on the energy partition, scale by scale, between kinetic, magnetic, and potential components in magnetic Archimedes Coriolis weak wave turbulence. Therefore, the results obtained in the present study are expected to be valid when the velocity amplitudes are weak in the sense that $u_0 \ll V_A$ and $u_0 \ll \ell_0\sqrt{f^2+N^2}$. Recall that the ratio u_0/ℓ_0 represents the eddy overturning time, V_A is the Alfvén speed, and f and N are the Coriolis parameter and the Brunt-Väisälä frequency, respectively.

With the aid of the potential induction scalar, which is a Lagrangian invariant for a diffusionless fluid, we have derived a dispersion relation [see Eq. (13)], characterizing both fast and slow MAC waves and generalizing previous studies. With respect to the case of magnetic Coriolis waves for which there are fast and slow modes (stable), stratification in the case of MAC waves acts to further reduce the propagation of slow modes and to further accelerate the propagation of fast modes. Similarities between our dispersion relation and that of f-plane magnetohydrodynamic shallow water waves have been drawn and briefly discussed invoking in particular the case of the solar tachocline. The derivation of the MHD shallow water equations by taking into account the equation for the induction potential scalar [see Eq. (3)] would allow one to analyze in more detail these similarities. It might be worth mentioning here that the analysis in this paper focuses on f planes so there are no Rossby modes in these wave spectra.

Based on additional analytical developments, we have analyzed in detail the effects of linear processes on the energy partition between the kinetic, magnetic, and potential components in the case of MAC wave turbulence considering either a diffusionless fluid or a diffusive fluid for which both magnetic and thermal Prandtl numbers are unity, for the sake of simplicity. Note that in some astrophysical flows, as the solar tachocline, high values of magnetic and hydrodynamic Reynolds numbers indicate that the effects of viscosity and magnetic diffusion are very low. In addition, at scale k^{-1}, where k is the radial (spherically average), the energy ratio such as kinetic/magnetic (called the Alfvén ratio) is the same considering either a diffusionless fluid or a diffusive fluid with $\nu = \eta = \kappa$.

In the case of magnetic Coriolis weak wave turbulence, it is found that, at large scales ($V_a k/f \ll 1$), the inertial waves affect the equipartition of energy between the kinetic and magnetic energy occurring in the nonrotating MHD turbulence submitted to a uniform magnetic field. The equipartition of energy is more affected by the inertial waves when the uniform magnetic field is parallel to the rotation axis ($\boldsymbol{B} \parallel \boldsymbol{\Omega}$, axisymmetric case). In fact, it has been demonstrated that the Alfvén ratio behaves like k^{-2} when $\boldsymbol{B} \parallel \boldsymbol{\Omega}$, in agreement with DNS data by Favier *et al.* [20], and as k^{-1} when $\boldsymbol{B} \perp \boldsymbol{\Omega}$ (asymmetric case). Also, the analysis of the one-dimensional spectrum in the vertical (x_3) direction in the axisymmetric case shows that, at large vertical scales ($V_A k_3/f \ll 1$), the Alfvén ratio behaves like k_3^{-2}. At small scales ($V_A k/f \gg 1$), the inertial waves do not affect the equipartition of energy between the magnetic and kinetic components occurring in the nonrotating MHD wave turbulence. The non-Alfvénic regime, which is due the nonlinear interactions and characterized by the fact that the Alfvén ratio is slightly smaller than one, cannot be captured by linear theory. According to linear theory, the inertial waves alter the dynamics of Alfvén waves at length scales ℓ such that $\ell \lesssim V_A/f$.

In the case of magnetic Archimedes weak wave turbulence, it is shown that, at large scales ($V_A k/N \ll 1$), there is an equipartition of energy between the magnetic and the potential components, and the energy ratio (potential/kinetic) exhibits a k^0 form and remains less than one. At small scales ($V_A k/N \gg 1$), gravity waves do not alter the equipartition of energy between magnetic and kinetic components induced by the linear dynamics of Alfvén waves and the energy ratio (potential/kinetic or potential/magnetic) behaves like k^{-1}. The effects of gravity waves, at small scales, appear to be very weak (see the bottom panel in Fig. 4).

When the Alfvén waves, inertial waves, and gravity waves are simultaneously present, the energy partition does not strongly differ from the case where the inertial waves are absent. In fact, at large scales $V_A k/\sqrt{N^2+f^2} \ll 1$, the energy ratios potential/magnetic and potential/kinetic exhibit a k^0 form, but there is no equipartition of energy between magnetic and potential components. At large scales, the effects of inertial waves are indicated by an increase of the kinetic energy and a decrease of potential and magnetic energies (see Figs. 4 and 5). At small scales, $V_A k/\sqrt{N^2+f^2} \gg 1$, the

simultaneous presence of gravity and inertial waves does not alter the equipartition of energy between magnetic and kinetic energy induced by the linear dynamic of the Alfvén waves, as already indicated. As in the case of magnetic Archimedes weak wave turbulence, at small scales, the potential energy is less important than the kinetic (or magnetic) energy and the energy ratio potential/kinetic behaves like k^{-1}.

We think that this work, which will be completed by performing direct numerical simulations and some analytical developments to characterize both weakly and strongly nonlinear interactions, would be useful for astrophysical applications especially for the solar tachocline, which supports huge-wavelength waves (up to 20% the diameter of the Sun), which oscillate once every couple of days [37].

APPENDIX A: A LINEAR SOLUTION FOR THE FOURIER MODES

1. Case of weak magnetic Coriolis wave turbulence

In nonstratified diffusionless electrically conducting fluid, the linear differential system Eq. (10) for the poloidal and toroidal modes of fluctuating velocity and magnetic fields reduces to

$$\underbrace{\begin{pmatrix}\dot{u}^{(1)}\\ \dot{u}^{(2)}\\ \dot{u}^{(3)}\\ \dot{u}^{(4)}\end{pmatrix}}_{\dot{\boldsymbol{v}}} = \underbrace{\begin{pmatrix}0 & \omega_R & \omega_A & 0\\ -\omega_R & 0 & 0 & -\omega_A\\ -\omega_A & 0 & 0 & 0\\ 0 & \omega_A & 0 & 0\end{pmatrix}}_{\mathbf{M_R}} \cdot \underbrace{\begin{pmatrix}u^{(1)}\\ u^{(2)}\\ u^{(3)}\\ u^{(4)}\end{pmatrix}}_{\boldsymbol{v}}, \tag{A1}$$

where $\omega_R = fk_3/k$ and $\omega_A = V_A k_3$ are the inertial and Alfvén frequencies, respectively. Equivalently, one can introduce the Green matrix $\mathbf{g}(t)$ such that $\mathbf{g}(t=0)$ is the 4×4 unit matrix and $\boldsymbol{v}(t) = \mathbf{g}(t)\cdot\boldsymbol{v}(0)$, so that $\dot{\mathbf{g}} = \mathbf{M}_R\cdot\mathbf{g}$. As indicated in Sec. III, the positive eigenvalues of the matrix $\mathbf{M}_R$ correspond to the frequencies ω_f and ω_s of fast and slow magnetic inertial waves described by Eq. (15).

The solution for $g_{ij}(t)$ $(i,j = 1,2,3,4)$ takes the form

$$\begin{aligned}
g_{11} &= g_{22} = \frac{\omega_f\cos(\omega_f t)+\omega_s\cos(\omega_s t)}{(\omega_f+\omega_s)},\\
g_{33} &= g_{44} = \frac{\omega_s\cos(\omega_f t)+\omega_f\cos(\omega_s t)}{(\omega_f+\omega_s)},\\
g_{12} &= -g_{21} = \frac{\omega_f\sin(\omega_f t)-\omega_s\sin(\omega_s t)}{(\omega_f+\omega_s)},\\
g_{34} &= -g_{43} = \frac{\omega_s\sin(\omega_f t)-\omega_f\sin(\omega_s t)}{(\omega_f+\omega_s)},\\
g_{13} &= g_{31} = g_{24} = g_{42} = \frac{(\cos(\omega_f t)-\cos(\omega_s t))\sqrt{\omega_f\omega_s}}{(\omega_f+\omega_s)},\\
g_{32} &= -g_{23} = g_{41} = -g_{14} = \frac{(\sin(\omega_f t)-\sin(\omega_s t))\sqrt{\omega_f\omega_s}}{(\omega_f+\omega_s)}.
\end{aligned} \tag{A2}$$

We note that when considering isotropic initial conditions, with a zero value for the cross-correlation between velocity and magnetic field fluctuations, the expression of the spectral density of kinetic and magnetic energies in terms of the elements g_{ij} can be expressed as

$$\begin{aligned}
\mathcal{E}_\kappa(\boldsymbol{k},t) &= \frac{S_\kappa(k,0)}{8\pi k^2}(|g_{\alpha\beta}|^2+\xi_m(k)|g_{\alpha\gamma}|^2),\\
\mathcal{E}_m(\boldsymbol{k},t) &= \frac{S_\kappa(k,0)}{8\pi k^2}(|g_{\gamma\alpha}|^2+\xi_m(k)|g_{\gamma\eta}|^2),
\end{aligned} \tag{A3}$$

where $(\alpha,\beta = 1,2)$ and $(\gamma,\eta = 3,4)$ and $\xi_m(k) = S_m(k,0)/S_\kappa(k,0)$. Recall that for a diffusive fluid with a unit value for the Prandtl magnetic number, the spectral density of energy is obtained by multiplying the one obtained for a diffusionless fluid by the factor $e^{-2\nu k^2 t}$.

2. Case of magnetic Archimedes weak wave turbulence

Without rotation, the differential linear system Eq. (10) reduces to

$$\underbrace{\begin{pmatrix}\dot{u}^{(1)}\\ \dot{u}^{(2)}\\ \dot{u}^{(3)}\\ \dot{u}^{(4)}\end{pmatrix}}_{\dot{\boldsymbol{v}}} = \underbrace{\begin{pmatrix}0 & 0 & \omega_A & 0\\ 0 & 0 & 0 & -\frac{\omega_{AG}^2}{\omega_A}\\ -\omega_A & 0 & 0 & 0\\ 0 & \omega_A & 0 & 0\end{pmatrix}}_{\mathbf{M}_G} \cdot \underbrace{\begin{pmatrix}u^{(1)}\\ u^{(2)}\\ u^{(3)}\\ u^{(4)}\end{pmatrix}}_{\boldsymbol{v}} + \begin{pmatrix}0\\ \pi^{(0)}\\ 0\\ 0\end{pmatrix}. \tag{A4}$$

As indicated previously, the toroidal modes $u^{(1)}$ and $u^{(3)}$ propagate with the Alfvén frequency, ω_A, while the poloidal modes $u^{(2)}$ and $u^{(4)}$ propagate with frequency $\omega_{AG} = \sqrt{\omega_A^2+\omega_G^2}$ characterizing the Alfvén gravity waves with $\omega_G = Nk_h/k$. The buoyancy mode $u^{(5)}$ also propagates with frequency ω_{AG} and satisfies the relation

$$\begin{aligned}
&\omega_G u^{(4)}(\boldsymbol{k},t)+\omega_A u^{(5)}(\boldsymbol{k},t)\\
&\quad = (\omega_A/\omega_G)\pi^{(0)} = \omega_G u^{(4)}(\boldsymbol{k},0)+\omega_A u^{(5)}(\boldsymbol{k},0),
\end{aligned} \tag{A5}$$

resulting from the fact that the induction potential scalar is a Lagrangian invariant for a diffusionless fluid [see Eq. (12)].

The positive eigenvalues of the matrix $\mathbf{M}_G$ are ω_A and ω_{AG} and the solution of the differential system of the Green matrix,

$$\dot{g}_{ij} = M_{in}g_{nj}+\Psi_{ij} \quad (i = 1,2,3,4)\ (j = 1,\ldots,5),$$

where the nonzero components of the matrix Ψ are $\psi_{24} = \omega_G^2/\omega_A$ and $\psi_{25} = \omega_G$, with the initial condition $g_{ij}(0) = \delta_{ij}$ is found as

$$\begin{aligned}
&g_{11} = g_{33} = \cos(\omega_A t), \quad g_{12} = g_{14} = g_{15} = 0,\\
&g_{13} = -g_{31} = \sin(\omega_A t), \quad g_{32} = g_{34} = g_{35} = 0,\\
&g_{22} = \cos(\omega_{AG} t), \quad g_{21} = g_{23} = 0, \quad g_{25} = \frac{\omega_G}{\omega_{AG}}\sin(\omega_{AG} t),\\
&g_{24} = -g_{42} = -\frac{\omega_A}{\omega_{AG}}\sin(\omega_{AG} t), \quad g_{41} = g_{43} = 0,\\
&g_{44} = \frac{\omega_G^2}{\omega_{AG}^2}+\frac{\omega_A^2}{\omega_{AG}^2}\cos(\omega_{AG} t),\\
&g_{45} = \frac{\omega_A\omega_G}{\omega_{AG}^2}[1-\cos(\omega_{AG} t)],\\
&g_{5j} = \delta_{5j}+\frac{\omega_G}{\omega_A}(\delta_{4j}-g_{4j}) \quad (j = 1,2,\ldots,5).
\end{aligned} \tag{A6}$$

For isotropic initial conditions with zero initial cross-correlation between velocity and magnetic (or density) field fluctuations, the expression of the spectral density of (kinetic, magnetic, or potential) energy (for a diffusionless fluid) is

$$\mathcal{E}_\kappa(\boldsymbol{k},t) = \frac{S_\kappa(k,0)}{8\pi k^2}(|g_{\alpha\beta}|^2 + \xi_m(k)|g_{\alpha\gamma}|^2 + \xi_p(k)|g_{5\alpha}|^2),$$
$$\mathcal{E}_m(\boldsymbol{k},t) = \frac{S_\kappa(k,0)}{8\pi k^2}(|g_{\gamma\alpha}|^2 + \xi_m(k)|g_{\gamma\eta}|^2 + \xi_p(k)|g_{5\eta}|^2), \tag{A7}$$
$$\mathcal{E}_p(\boldsymbol{k},t) = \frac{S_\kappa(k,0)}{8\pi k^2}(|g_{5\alpha}|^2 + \xi_m(k)|g_{5\eta}|^2 + \xi_p(k)|g_{55}|^2),$$

where $\xi_p(k) = S_p(k,0)/S_\kappa(k,0)$. As already indicated, for a diffusive fluid with a unit value for the magnetic Prandtl number, the spectral density of energy is obtained by multiplying the one obtained for a diffusionless fluid by the factor $e^{-2\nu k^2 t}$.

3. Case of magnetic Archimedes Coriolis weak wave turbulence

For a diffusionless fluid, the differential system Eq. (10) characterizes the linear dynamics of magnetic-inertia-gravity weak wave turbulence. Because in the present study we have considered initial isotropic conditions with a zero value for the initial magnetic and potential energies and also for the initial cross-correlation between velocity and magnetic (or density) field fluctuations, we report here only the solution for the components $g_{\alpha\eta}(\alpha = 1,2,\ldots,5)$ and $(\eta = 1,2)$,

$$g_{11} = \frac{(\omega_F^2 - \omega_{AG}^2)}{(\omega_F^2 - \omega_S^2)}\cos(\omega_F t) - \frac{(\omega_S^2 - \omega_{AG}^2)}{(\omega_F^2 - \omega_S^2)}\cos(\omega_S t),$$
$$g_{12} = -g_{21} = \frac{\omega_R}{(\omega_F^2 - \omega_S^2)}[\omega_F \sin(\omega_F t) - \omega_S \sin(\omega_S t)],$$
$$g_{22} = \frac{(\omega_{AG}^2 + \omega_R^2 - \omega_S^2)}{(\omega_F^2 - \omega_S^2)}\cos(\omega_F t) - \frac{(\omega_{AG}^2 + \omega_R^2 - \omega_F^2)}{(\omega_F^2 - \omega_S^2)}\cos(\omega_S t),$$
$$g_{31} = -\frac{(\omega_F^2 - \omega_{AG}^2)}{(\omega_F^2 - \omega_S^2)}\frac{\omega_A}{\omega_F}\sin(\omega_F t) + \frac{(\omega_S^2 - \omega_{AG}^2)}{(\omega_F^2 - \omega_S^2)}\frac{\omega_A}{\omega_S}\sin(\omega_S t), \tag{A8}$$
$$g_{32} = -\frac{(\omega_S^2 - \omega_{AG}^2 - \omega_R^2)}{(\omega_F^2 - \omega_S^2)}\frac{(\omega_F^2 - \omega_{AG}^2 - \omega_R^2)}{\omega_R\omega_A}\cos(\omega_F t) + \frac{(\omega_F^2 - \omega_{AG}^2 - \omega_R^2)}{(\omega_F^2 - \omega_S^2)}\frac{(\omega_S^2 - \omega_{AG}^2 - \omega_R^2)}{\omega_R\omega_A}\cos(\omega_S t),$$
$$g_{41} = \frac{\omega_A\omega_R}{(\omega_F^2 - \omega_S^2)}[\cos(\omega_F t) - \cos(\omega_S t)],$$
$$g_{42} = -\frac{(\omega_S^2 - \omega_{AG}^2 - \omega_R^2)}{(\omega_F^2 - \omega_S^2)}\frac{\omega_A}{\omega_F}\sin(\omega_F t) + \frac{(\omega_F^2 - \omega_{AG}^2 - \omega_R^2)}{(\omega_F^2 - \omega_S^2)}\frac{\omega_A}{\omega_S}\sin(\omega_S t),$$

where the fast and slow frequencies ω_F and ω_S are described by Eq. (19).

APPENDIX B: TIME DEVELOPMENT OF KINETIC AND MAGNETIC ENERGIES IN (AXISYMMETRIC) MAGNETIC CORIOLIS WEAK WAVE TURBULENCE

To determine the kinetic and magnetic energies per unit mass, $E_\kappa(t) = \int_0^\infty S_\kappa(k,t)dk$ and $E_m(t) = \int_0^\infty S_m(k,t)dk$, we use the following form for the initial radial spectrum $S_\kappa(k,0)$:

$$S_\kappa(k,0) = 4E_\kappa(0)\pi^{-\frac{1}{2}}k_0^{-3}k^2 e^{-k_c^{-2}k^2}, \tag{B1}$$

with k_0 the peak wave number, consistent with the observed spectrum in most experiments or DNS [46]. The time development of kinetic and magnetic energies in the case of MC weak wave turbulence are determined by integrating numerically the spectrum Eq. (36) over the radial wave number. In addition, we compute analytically the short-time and the long-time approximations of these energies.

Short-time approximations of energies can be derived by using the series representation of the function $\sin(t\sqrt{D_0})$ in Eq. (36) at $ft\sqrt{1+4\mathcal{L}_k^2} \ll 1$. The result is

$$\frac{E_\kappa(t)}{E_\kappa(0)} = 1 - 3\nu k_c^2 t - \frac{1}{2}V_A^2 k_0^2 t^2 + \frac{5}{2}\nu k_0^4 V_A^2 t^3 + \frac{1}{4}\left[\frac{1}{10}f^2(V_A k_0)^2 + V_A^4 k_c^4\right]t^4 - \ldots,$$
$$\frac{E_m(t)}{E_\kappa(0)} = \frac{1}{2}V_A^2 k_0^2 t^2 - \frac{5}{2}\nu k_0^4 V_A^2 t^3 - \frac{1}{4}\left[\frac{1}{10}f^2(V_A k_0)^2 + V_A^4 k_c^4\right]t^4 - \ldots. \tag{B2}$$

Regarding the development of the kinetic energy, the above short-time approximations indicate that the most dominant corrective term is of order $O(t)$ and is due to viscosity effects, while for the magnetic energy, which is zero at $t = 0$, the dominant term is of order $O(t^2)$ and is due to the imposed Alfvén speed. Therefore, the Alfvén ratio $E_\kappa(t)/E_m(t)$ behaves like t^{-2}. Note that the rotation effects represented by f appear only in higher-order corrections of $O(t^4)$. Figure 6 shows the time-history, $0 \leqslant t^+ = (u_0\ell_0)t \leqslant 5$, of $E_\kappa(t^+)/E_\kappa(0)$ and $E_m(t^+)/E_\kappa(0)$ with the Elsasser number, $\Lambda = V_A/(f\eta)$, as the variable parameter, while Fig. 7 shows the time-history of the Alfvén ratio $E_\kappa(t^+)/E_m(t^+)$.

The LST results with $k_0 = 3$ (case where $(f \neq 0, V_A \neq 0)$) or $k = 6.8$ (case where $(f = 0, V_A \neq 0)$) are displayed in top panels, whereas the DNS results are displayed in bottom panels. As expected, there is a quantitative agreement between the DNS results and LST ones, in the sense that both results show that the magnetic fluctuations are damped by rotation as Λ increases.

Without rotation ($\Lambda \to \infty$), the magnetic energy grows with time (like $V_A^2 t^2$, as already indicated) during an initial phase, reaches a maximum value and after decays, as time elapses. As for the kinetic energy, it decays with time. According to LST, the decay of the magnetic energy is accompanied by an equipartition of energy (between the magnetic and kinetic components), so that the Alfvén ratio

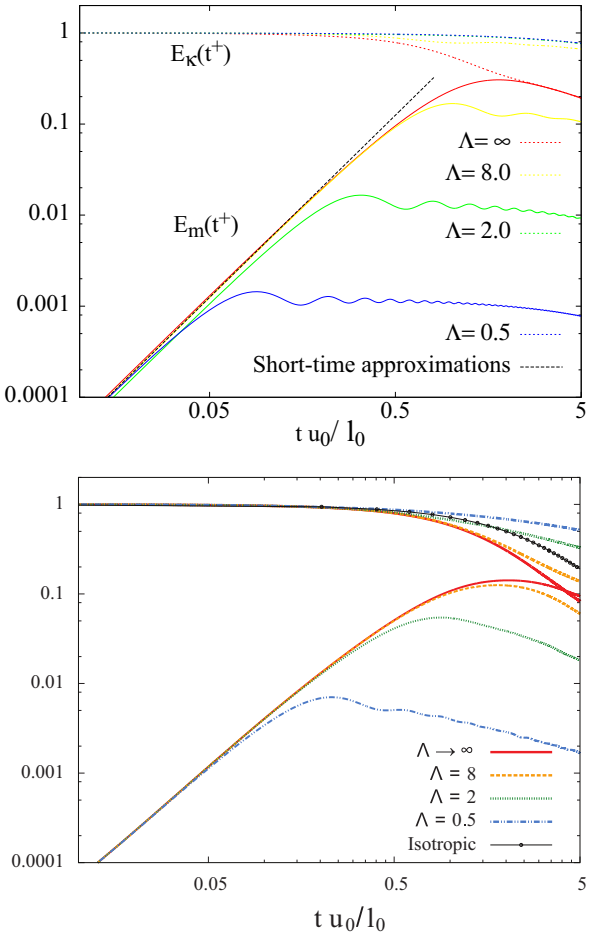

FIG. 6. Time history of kinetic and magnetic energies normalized by the initial kinetic energy in a rotating homogeneous turbulence submitted to a uniform magnetic field aligning with the rotation axis (axisymmetric case) for several values of the Elsasser number, $\Lambda = 0.5, 2.0, 8.0, \infty$ (nonrotating case). Top panel: LST results. Bottom panel: DNS results by Favier *et al.* [20].

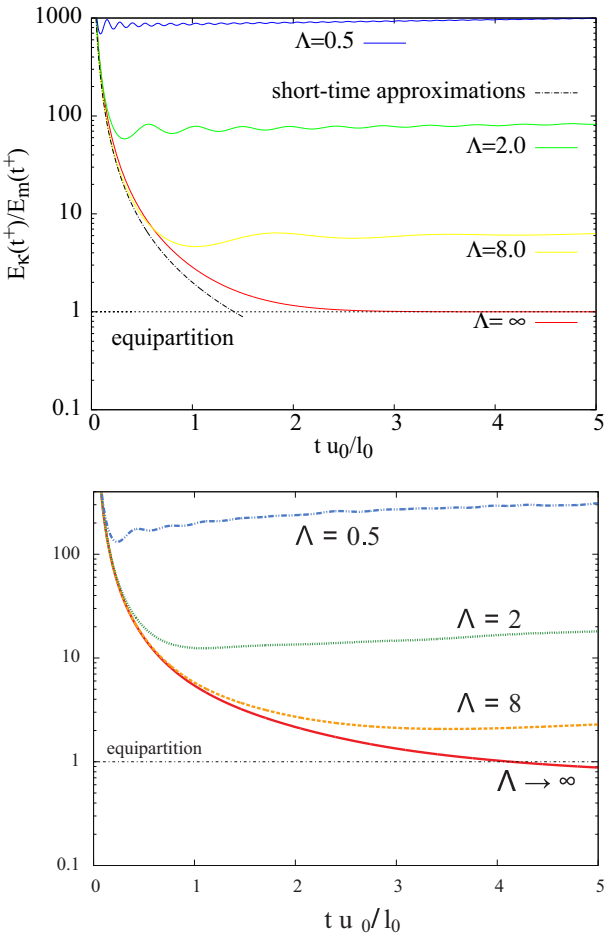

FIG. 7. Time history of the Alfvén ratio $E_\kappa(t^+)/E_m(t^+)$ in a rotating homogeneous turbulence submitted to a uniform magnetic field aligning with the rotation axis (axisymmetric case) for several values of the Elsasser number, $\Lambda = 0.5, 2.0, 8.0, \infty$ (nonrotating case). Top panel: LST results. Bottom panel: DNS results by Favier *et al.* [20].

is unity,

$$E_\kappa(t) = E_m(t) \sim \frac{E_\kappa(0)}{2\left(2\eta k_0^2 t\right)^{\frac{3}{2}}}, \quad \eta k_0^2 t \gg 1.$$

This behavior rather characterizes a wave turbulence regime for which $V_A \gg u_0$, where u_0 is the characteristic velocity of eddy, as indicated at the beginning of Sec. IV. In counterpart, for a strong MHD turbulence regime ($V_A \sim u_0$), the Alfvén ratio is slightly smaller than one, indicating the presence of non-Alfvénic fluctuations which cannot be captured by LST [20,25–27].

In the presence of rotation ($f \neq 0, V_A \neq 0$), the inertial waves modify the dynamics of Alfvén waves especially at large scales as discussed in Sec. IV. This is signaled by the fact that, with respect to the case where $f = 0$, the initial phase during which the magnetic energy grows is reduced (more and more as rotation rate increases) and the kinetic energy decay rate is also reduced. A consequence of the inertial wave effects on the dynamic of Alfvèn waves is that the equipartition of energy (between magnetic and kinetic components) is broken, as it can be deduced from the following relations giving the long-time behavior of energies for both a diffusionless fluid ($\nu = 0$ and $\eta = 0$),

$$\begin{aligned} \frac{E_\kappa(t)}{E_\kappa(0)} &= \left[1 - 3\left(\frac{V_A k_0}{f}\right)^2 + \ldots\right], \\ \frac{E_m(t)}{E_\kappa(0)} &= \left[3\left(\frac{V_A k_0}{f}\right)^2 - \ldots\right], \end{aligned} \tag{B3}$$

and a diffusive fluid with $\nu = \eta$,

$$\begin{aligned} \frac{E_\kappa(t)}{E_\kappa(0)} &= \left(2\eta k_0^2 t\right)^{-\frac{3}{2}} - 3\left(\frac{V_A k_0}{f}\right)^2 \left(2\eta k_0^2 t\right)^{-\frac{5}{2}} + \ldots, \\ \frac{E_m(t)}{E_\kappa(0)} &= 3\left(\frac{V_A k_0}{f}\right)^2 \left(2\eta k_0^2 t\right)^{-\frac{5}{2}} - \ldots. \end{aligned} \tag{B4}$$

Note that the above long-time approximations have been derived assuming that, at large time, the important contribution to the spectrum Eq. (36) comes from the part $(D_1/D_0)e^{-2\nu k^2 t}$,

and hence the contribution of the damped oscillating part $[D_2 \sin(t\sqrt{D_0})/(D_0 t\sqrt{D_0})]e^{-2\nu k^2 t}$ is omitted.

APPENDIX C: DEVELOPMENT OF THE ALFVÉN RATIO IN FUNCTION OF THE VERTICAL WAVE NUMBER IN (AXISYMMETRIC) MAGNETIC CORIOLIS WAVE TURBULENCE

The one-dimensional spectrum in the vertical (x_3) direction of kinetic energy in the case of the (axisymmetric) magnetic Coriolis weak wave turbulence can be written as

$$\mathcal{S}_\kappa(k_3,t) = \iint_{-\infty}^{+\infty} \mathcal{E}_\kappa(\boldsymbol{k},t)dk_1dk_3 = \pi \int_0^\infty \mathcal{E}_\kappa(\boldsymbol{k},t)dk_h^2, \tag{C1}$$

where $\mathcal{E}_\kappa(\boldsymbol{k},t)$ is described by Eq. (33). Equation (B1) is used for the initial spectrum $S_\kappa(k,0)$, and the integral with respect to the horizontal wave number, $0 < k_h < \infty$, is performed numerically. It is found that, at large dimensionless time ft, the Alfvén ratio exhibits an oscillatory behavior around $[1 + (2V_A^2k_3^2/f^2)^{-1}]$ (see Fig. 2). In this appendix, we propose to determine this limit.

We ignore the oscillating part in the expression of the spectral density of kinetic energy, so that

$$\mathcal{E}_\kappa(k_3,k_h,t) = \frac{S_\kappa(k,0)}{4\pi k_3^2(1+\alpha^2)}\left[\frac{1+2\mathcal{L}_{k_\parallel}^2(1+\alpha^2)}{1+4\mathcal{L}_{k_\parallel}^2(1+\alpha^2)}\right] \times \exp\left[-2\nu k_3^2 t(1+\alpha^2)\right], \tag{C2}$$

in which $\mathcal{L}_{k_\parallel} = V_A k_3/f$ and $\alpha = k_h/k_3$. Accordingly, the substitution of this form into Eq. (C1) gives

$$\mathcal{S}_\kappa(k_3,t) = C(k_3)\int_0^\infty \frac{\left(1+2\mathcal{L}_{k_\parallel}^2\right)+2\mathcal{L}_{k_\parallel}^2 y}{\left(1+4\mathcal{L}_{k_\parallel}^2\right)+4\mathcal{L}_{k_\parallel}^2 y}e^{-\beta y}dy,$$

where $\beta = (k_3^2/k_0^2 + 2\nu k_3^2 t)$ and $C(k_3)$ is a function of the vertical wave number that is not necessary to specify it here. The latter integral can be determined analytically,

$$\mathcal{S}_\kappa(k_3,t) = \frac{C(k_3)}{2}\left[\frac{1}{\beta} + (\chi-1)\mathbf{E}_i(-\beta\chi)\mathrm{e}^{\beta\chi}\right], \tag{C3}$$

where

$$\chi = \frac{1+4\mathcal{L}_{k_\parallel}^2}{4\mathcal{L}_{k_\parallel}^2},$$

and $\mathbf{E}_i(-\beta\chi)$ is the exponential integral function [47]. By using the asymptotic representations of $\mathbf{E}_i(-\beta\chi)$, we obtain

$$\mathcal{S}_\kappa(k_3,t) = \frac{C(k_3)}{2}\left\{\frac{1}{\beta} + (\chi-1)\left[\sum_{m=1}^{n}(-1)^m\frac{(m-1)!}{(\beta\chi)^m} + R_n\right]\right\}, \tag{C4}$$

where $|R_n| < \frac{n!}{(\beta\chi)^{n+1}}$ [47]. The expression of $\mathcal{S}_m(k_3,t)$ is deduced from the relation

$$\mathcal{S}_\kappa(k_3,t) + \mathcal{S}_m(k_3,t) = C(k_3)\beta^{-1},$$

so that

$$\lim_{ft\to\infty}\frac{\mathcal{S}_\kappa(k_3,t)}{\mathcal{S}_m(k_3,t)} = 1 + \frac{1}{2\mathcal{L}_{k_\parallel}^2} = 1 + \frac{f^2}{2V_A^2k_3^2}. \tag{C5}$$

APPENDIX D: DEVELOPMENT, SCALE BY SCALE, OF THE ALFVÉN RATIO IN (ASYMMETRIC) MAGNETIC CORIOLIS WAVES TURBULENCE

In this appendix, we report the detail of calculations leading to the relation Eq. (41) that gives the long-time limit of the Alfvén ratio $S_\kappa(k,t)/S_m(k,t)$ in the case of asymmetric magnetic-inertial weak wave turbulence (i.e., case where the uniform magnetic field is perpendicular to the system rotation axis). In that case, the frequencies ω_R and ω_A are

$$\omega_R = 2\Omega\cos\theta, \quad \omega_A = V_A\sin\theta\cos\varphi,$$

where θ and φ are, respectively, the polar and azimuthal angles in the spherical coordinates system for the wave vector $\boldsymbol{k}$, as indicated in Sec. III.

At large dimensionless time $2\Omega t \gg 1$, the dominant contribution to the radial spectrum of kinetic and magnetic energies comes from the steady part,

$$\frac{S_\kappa(k,t)}{S_\kappa(k,0)} \simeq \frac{1}{4\pi}\int_0^\pi \underbrace{\left[\int_0^{2\pi}\frac{\omega_R^2+2\omega_A^2}{\omega_R^2+4\omega_A^2}d\varphi\right]}_{J(k,\theta)}\sin\theta d\theta. \tag{D1}$$

We set $\omega_{Ah} = V_A\sin\theta$, so that

$$J(k,\theta) = \pi + \frac{\omega_R^2}{2\left(\omega_R^2+2\omega_{Ah}^2\right)}\int_0^{2\pi}\frac{d\alpha}{1+\frac{2\omega_{Ah}^2}{\omega_R^2+2\omega_{Ah}^2}\cos\alpha} = \pi\left[1+\frac{\omega_R}{\sqrt{\omega_R^2+4\omega_{Ah}^2}}\right], \tag{D2}$$

and hence

$$\int_0^\pi J(k,\theta)\sin\theta d\theta = 2\pi\left[1+\left(\frac{f}{2V_Ak}\right)\int_0^1\frac{\beta y}{\sqrt{y^2+\beta^2}}dy\right] = 2\pi\left[1+\frac{f}{f+4V_Ak}\right], \tag{D3}$$

where $\beta^2 = 4(V_Ak)^2/[f^2-4(V_Ak)^2]$. Therefore, the long-time limit of the radial spectrum takes the form

$$\lim_{ft\to\infty}\frac{S_\kappa(k,t)}{S_\kappa(k,0)} = \frac{1}{2}\left[1+\frac{f}{f+4V_Ak}\right], \quad \lim_{ft\to\infty}\frac{S_m(k,t)}{S_\kappa(k,0)} = \frac{1}{2}\left[1-\frac{f}{f+4V_Ak}\right], \tag{D4}$$

and thus the Alfvén ratio behaves like

$$\lim_{ft\to\infty}\frac{S_\kappa(k,t)}{S_m(k,t)} = 1 + 2\frac{f}{4(V_Ak)} = 1 + \frac{1}{2\mathcal{L}_k}. \tag{D5}$$

Therefore, at large scales ($V_Ak/f \ll 1$), the Alfvén ratio behaves like k^{-1}, while at small scales ($V_Ak/f \gg 1$), there is an equipartition of energy between kinetic and magnetic components.

[1] R. Hide, Free hydromagnetic oscillations of the Earth's core and the theory of the geomagnetic secular variation, Philos. Trans. R. Soc. London A: Math. Phys. Eng. Sci. **259**, 615 (1966).

[2] P. Kumar, S. Talon, and J.-P. Zahn, Angular momentum transport by gravity waves and its effect on the rotation of the solar interior, Astrophys. J. **520**, 859 (1999).

[3] P. H. Roberts and A. M. Soward, Magnetohydrodynamics of the Earth's core, Annu. Rev. Fluid Mech. **4**, 117 (1972).

[4] H. K. Moffatt, *Field Generation in Electrically Conducting Fluids* (Cambridge University Press, Cambridge/London/New York/Melbourne, 1978).

[5] C. C. Finlay, Waves in the presence of magnetic fields, rotation, and convection, in *Dynamos*, Vol. LXXXVIII of Lecture Notes of the Les Houches Summer School, edited by P. Cardin and L. Cugliandolo (Elsevier, New York, 2008), Chap. 8.

[6] M. D. Nornberg, H. Ji, E. Schartman, A. Roach, and J. Goodman, Observation of Magnetocoriolis Waves in a Liquid Metal Taylor-Couette Experiment, Phys. Rev. Lett. **104**, 074501 (2010).

[7] S. A. Balbus and J. F. Hawley, A powerful local shear instability in weakly magnetized disks. I-Linear analysis, Astrophys. J. **376**, 214 (1991).

[8] D. R. Sisan, W. L. Shew, and D. P. Lathrop, Lorentz force effects in magneto-turbulence, Phys. Earth Planet. Inter. **135**, 137 (2003).

[9] F. Stefani, T. Gundrum, G. Gerbeth, G. Rüdiger, M. Schultz, J. Szklarski, and R. Hollerbach, Experimental Evidence for Magnetorotational Instability in a Taylor-Couette Flow under the Influence of a Helical Magnetic Field, Phys. Rev. Lett. **97**, 184502 (2006).

[10] A. Salhi, T. Lehner, F. Godeferd, and C. Cambon, Magnetized stratified rotating shear waves, Phys. Rev. E **85**, 026301 (2012).

[11] J. Pedlosky, *Geophysical Fluid Dynamics* (Springer Science & Business Media, Berlin, 2013).

[12] A. M. Soward and E. Dormy, *Mathematical Aspects of Natural Dynamos* (CRC Press, Boca Raton, 2007).

[13] S. I. Braginsky, Magnetic waves in the Earth's core, Geomag. Aeron. **7**, 1050 (Engl. transl. 851–859) (1967).

[14] P. A. Gilman, Magnetohydrodynamic "shallow water" equations for the solar tachocline, Astrophys. J. **544**, L79 (2000).

[15] D. A. Schecter, J. F. Boyd, and P. A. Gilman, "Shallow-Water" Magnetohydrodynamic Waves in the Solar Tachocline, Astrophys. J. **551**, L185 (2001).

[16] T. V. Zaqarashvili, R. Oliver, J. L. Ballester, and B. M. Shergelashvili, Rossby waves in "shallow water" magnetohydrodynamics, Astron. Astrophys. **470**, 815 (2007).

[17] K. Heng and A. Spitkovsky, Magnetohydrodynamic shallow water waves: Linear analysis, Astrophys. J. **703**, 1819 (2009).

[18] V. Zeitlin, Remarks on rotating shallow-water magnetohydrodynamics, Nonlin. Proc. Geophys. Eur. Geosci. Union **20**, 893 (2013).

[19] D. O. Gough, An introduction to the solar tachocline, in *The Solar Tachocline*, edited by David W. Hughes, Robert Rosner, and Nigel O. Weiss (Cambridge University Press, Cambridge, 2007).

[20] B. Favier, F. Godeferd, and C. Cambon, On the effect of rotation on magnetohydrodynamic turbulence at high magnetic Reynolds number, Geophys. Astrophys. Fluid Dyn. **106**, 89 (2012).

[21] P. A. Davidson, *An Introduction to Magnetohydrodynamics* (Cambridge University Press, Cambridge, 2013).

[22] R. H. Kraichnan, Inertial-Range spectrum of hydomagnetic turbulence, Phys. Fluids **8**, 1385 (1965).

[23] N. Gillet, D. Jault, E. Canet, and A. Fournier, Fast torsional waves and strong magnetic field within the Earth's core, Nature **465**, 74 (2010).

[24] C. C. Finlay, M. Dumberry, A. Chulliat, and M. A. Pais, Short timescale core dynamics: Theory and observations, Space Sci. Rev. **155**, 177 (2010).

[25] W. K. Matthaeus and M. L. Goldstein, Measurement of the rugged invariants of magnetohydrodynamic turbulence in the solar wind, J. Geophys. Res. **87**, 6011 (1982).

[26] J. C. Perez and S. Boldyrev, On weak and strong magnetohydrodynamic turbulence, Astrophys. J. **672**, L61 (2008).

[27] B. Bigot, S. Galtier, and H. Politano, Development of anisotropy in incompressible magnetohydrodynamic turbulence, Phys. Rev. E **78**, 066301 (2008).

[28] H. Moffatt, Turbulent dynamo action at low magnetic Reynolds number, J. Fluid Mech. **41**, 435 (1971).

[29] G. K. Batchelor and I. Proudman, The effect of rapid distortion of a fluid in turbulent motion, Q. J. Mech. Appl. Math. **7**, 83 (1954).

[30] A. A. Townsend, *The Structure of Turbulent Shear Flow* (Cambridge University Press, Cambridge, 1976).

[31] A. Salhi and C. Cambon, On the stability of rotating stratified shear flow: An analytical study, Phys. Rev. E **81**, 026302 (2010).

[32] J. R. Herring, Approach of axisymmetric turbulence to isotropy, Phys. Fluids **17**, 859 (1974).

[33] P. Sagaut and C. Cambon, *Homogeneous Turbulence Dynamics* (Cambridge University Press, Cambridge, 2008).

[34] G. Barnes, K. B. MacGregor, and P. Charbonneau, Gravity waves in a magnetized shear layer, Astrophys. J. **498**, L169 (1998).

[35] A. Salhi and A. Pieri, Wave-vortex mode coupling in neutrally stable baroclinic flows, Phys. Rev. E **90**, 043003 (2014).

[36] H. Hanazaki, Linear processes in stably and unstably stratified rotating turbulence, J. Fluid Mech. **465**, 157 (2002).

[37] S. Hunter, Waves in shallow water magnetohydrodynamics, PhD thesis, University of Leeds, Faculty of Maths and Physical Sciences, School of Mathematics, Applied Mathematics, 2015.

[38] T. D. Ringler and D. A. Randall, A potential enstrophy and energy conserving numerical scheme for solution of the shallow-water equations on a geodesic grid, Monthly Weather Rev. **130**, 1397 (2002).

[39] S. H. Derbyshire and J. C. R. Hunt, Structure of turbulence in stably stratified atmospheric boundary layers: Comparison of large eddy simulations and theoretical results, in *Waves and Turbulence in Stably Stratified Flows*, edited by S. D. Mobbs and J. C. King (Clarendon Press, London, 1993), pp. 23–59.

[40] A. Salhi and C. Cambon, Anisotropic phase-mixing in homogeneous turbulence in a rapidly rotating or in a strongly stratified fluid: An analytical study, Phys. Fluids **19**, 055102 (2007).

[41] B. Lehnert, The decay of magnetoturbulence in the presence of a magnetic field and Coriolis force, Q. Appl. Math. **12**, 321 (1955).

[42] P. Piccirillo and C. W. van Atta, The evolution of a uniformly sheared thermally stratified turbulent flow, J. Fluid Mech. **334**, 61 (1997).

[43] A. Brandenburg, T. Kahniashvili, and A. G. Tevzadze, Nonhelical Inverse Transfer of a Decaying Turbulent Magnetic Field, Phys. Rev. Lett. **114**, 075001 (2015).

[44] G. K. Batchelor, *The Theory of Homogeneous Turbulence* (Cambridge University Press, Cambridge, 1953).

[45] E. J. Hinch, *Perturbation Methods* (Cambridge University Press, Cambridge, 1991).

[46] H. Hanazaki and J. C. R. Hunt, Linear processes in unsteady stably stratified turbulence, J. Fluid Mech. **318**, 303 (1996).

[47] I. S. Gradshteyn and I. M. Ryzhik, *Table of Integrals, Series, and Products* (Academic Press, San Diego, 2014).